Revisiting carbon isotope discrimination in C_3 plants shows respiration rules when photosynthesis is low

Florian A. Busch[1,*], Meisha Holloway-Phillips[1,2], Hilary Stuart-Williams[1] and Graham D. Farquhar[1]

[1]Research School of Biology and ARC Centre of Excellence for Translational Photosynthesis, Australian National University, Acton ACT 2601, Australia
[2]Current address: Department of Environmental Sciences, University of Basel, 4056 Basel, Switzerland

Author ORCID IDs:
Florian A. Busch: 0000-0001-6912-0156; Meisha Holloway-Phillips: 0000-0002-8353-3536; Hilary Stuart-Williams: 0000-0002-9272-9178; Graham D. Farquhar: 0000-0002-7065-1971

Short title: Revised C_3 carbon isotope discrimination model

* Corresponding author:
Florian Busch
Plant Science Division
Research School of Biology
46 Sullivans Creek Road
The Australian National University
Acton, ACT, 2601
Australia

Tel: +61 2 6125 0123
Email: florian.busch@anu.edu.au

Key words

Carbon isotope discrimination, mesophyll conductance, CO_2 diffusion, photosynthesis model

Abstract

Stable isotopes are commonly used to study the diffusion of CO_2 inside photosynthetic tissues of plants. The standard method to interpret the observed preference for the lighter carbon isotope in C_3 photosynthesis involves the model by Farquhar, O'Leary and Berry, which relates carbon isotope discrimination to physical and biochemical processes inside the leaf. However, under many conditions the model returns unreasonable results for mesophyll conductance to CO_2 diffusion (g_m), especially when rates of photosynthesis are low. Here we re-derive the carbon isotope discrimination model using modified assumptions related to the isotope effect of mitochondrial respiration. In particular, we treat the carbon pool associated with respiration as separate from the pool of the primary assimilates. We experimentally test the model by comparing g_m values measured with different CO_2 source gases varying in their isotopic composition and show that our new model returns matching g_m values that are much more reasonable than those obtained with the old model. We use our results to discuss CO_2 diffusion properties inside the mesophyll.

Introduction

Plant carbon exchange with the atmosphere is central to our understanding of diverse fields ranging from agriculture and ecology to global climate. Measurements of CO_2 fluxes between plant and atmosphere using standard portable gas exchange equipment[1] have been increasingly coupled with isotopic analyses as the technology of isotope ratio mass spectrometers and optical isotope analyzers has advanced. Isotopologues, molecules that differ

54 only in their isotopic composition, vary in the speed at which they diffuse or get processed in
55 biochemical reactions, and thereby carry information about these same processes. Carbon
56 isotope data have thus enabled us to separate photosynthesis from respiratory fluxes that
57 occur simultaneously in the leaf[2,3] and to identify genotypes differing in water-use efficiency[4].
58 They have helped us to understand the ecological impacts of different photosynthetic
59 pathways[5] and to quantify the biosphere's contribution to the global carbon cycle[6,7]. The
60 analysis of carbon isotopes and how plants discriminate between them has therefore become
61 one of the most important tools available for studying the physiology of plants and how they
62 interact with their environment.

63 Underlying all these uses are mathematical models that relate the isotopic composition
64 of a sample to a biochemical or physical process so that measurements can be compared to
65 predictions. At the leaf level, the process by which photosynthesis modifies the carbon isotopic
66 composition of the surrounding air was related to C_3 leaf biochemistry with the model of
67 Farquhar, et al. [8], which has become the standard description of photosynthetic carbon isotope
68 discrimination. Subsequently, properties of the internal diffusion of CO_2 from the intercellular
69 space to the chloroplast have been derived[9,10] and the impacts of heterotrophic respiration[11]
70 and refixation of respired CO_2 in sink tissues[12] on photosynthetic isotope discrimination have
71 been described and incorporated into the model.

72 In addition to estimating the intrinsic water-use-efficiency (the ratio of CO_2 assimilation
73 rate to stomatal conductance) of plants from the isotopic composition of bulk leaf material, the
74 carbon isotope discrimination model is also widely employed to assess mesophyll diffusive
75 properties from online measurements. It has been difficult, however, to observe consistent

trends in leaf-level measurements of the mesophyll conductance to CO_2 diffusion (g_m), and values estimated from carbon isotope data often do not match those measured by other methods[13]. This is especially true when measurements are taken close to the compensation point, where mitochondrial respiration (R_d) is large relative to the net CO_2 assimilation rate (A). Approaching the CO_2 compensation point, measurements with isotopic methods often result in increasing g_m values, while chlorophyll fluorescence methods generally show decreases in g_m [14-17]. In addition, estimates of g_m are strongly affected by the assumptions made regarding the values of the fractionation factors that the isotope discrimination model relies on, again introducing the largest uncertainties close to the compensation point. As a result, our confidence in the estimated values of g_m is currently insufficient to assess the fundamental nature of CO_2 diffusion inside the leaf. With the arrival of high-precision, high-throughput isotope measurement equipment these uncertainties have become less likely a result of measurement inaccuracies, and point towards insufficiencies in the parameterization of the isotope discrimination model itself. A close examination of the respiratory component reveals that the current model does not represent the respiratory biochemistry of the leaf well, which is affecting the predicted isotope composition of the assimilates.

Here, we re-derive the carbon isotope discrimination model using assumptions regarding respiration that are different from the model of Farquhar, et al. [8], resulting in changes that have important implications for quantifying diffusive resistances inside the leaf. We assess this model with carbon isotope discrimination data obtained with source gases of different carbon isotope composition, which allows us to assess the quality of the model independently of the parameter values used in it. Our results indicate that g_m values derived with the new

model are more reliable than those obtained with the old model, especially under conditions where R_d is large relative to A, and do not depend on the source gas used.

The basis of carbon isotope discrimination

Photosynthetic CO_2 uptake in plants requires the diffusion of CO_2 from the air surrounding the leaf through the boundary layer of the leaf, through the stomata into the intercellular air space (IAS), and on through the mesophyll into the chloroplast, where it is assimilated by Rubisco. The widely-used photosynthetic model of Farquhar, et al. [18] relies on the chloroplastic CO_2 concentration (C_c) as a key input parameter in determining the CO_2 uptake of the leaf. According to Fick's law of diffusion, the net CO_2 uptake by the plant (A; in µmol m^{-2} s^{-1}) is equal to the product of the CO_2 gradient and the associated conductance for CO_2 diffusion (ignoring for the moment ternary effects):

$$A = \left(C_a - C_s\right) g_{bl} = \left(C_s - C_i\right) g_s = \left(C_i - C_c\right) g_m \,, \qquad (1)$$

where C_a, C_s, and C_i are the CO_2 concentrations in the ambient air, at the leaf surface, and the IAS (in µmol mol^{-1}), respectively. The conductances across the boundary layer, the stomata, and the mesophyll are denoted g_{bl}, g_s, and g_m (in mol m^{-2} s^{-1}). Accordingly, C_c can be calculated from A and C_a knowing the conductances along the diffusion pathway of CO_2. While g_{bl} is usually large in gas exchange systems and g_s can be easily estimated from the transpiration rate of the leaf using the same gas exchange equipment, measurements of g_m are less straightforward. Several methods have been developed to estimate g_m, each requiring different assumptions and thus having different advantages and disadvantages[19]. Two commonly used techniques combine measurements of gas exchange with either measurements of the photosynthetic

electron transport rate (J_a; assessed by chlorophyll fluorescence)[20-22], or with instantaneous carbon isotope discrimination[9]. The carbon isotope discrimination method is based on the theory that the more common lighter CO_2 isotopologue ($^{12}CO_2$) diffuses more rapidly than the heavier $^{13}CO_2$, and with a proportionally even greater reactivity with the CO_2-fixing enzyme Rubisco, resulting in a discrimination against $^{13}CO_2$. Advances in laser instrumentation have made it possible to instantaneously measure the (observed) discrimination (Δ_{obs}^{13}) together with standard gas exchange measurements, from which the mesophyll conductance can be deduced.

The original model for ^{13}C discrimination[8] has been extended to include ternary effects[23], which in its full notation can be written as:

$$\Delta^{13} = \frac{1}{1-t}\left[a_b\frac{C_a - C_s}{C_a} + a_s\frac{C_s - C_i}{C_a}\right] + \frac{1+t}{1-t}\left[a_m\frac{C_i - C_c}{C_a} + b\frac{C_c}{C_a} - \frac{R_d}{A+R_d}\frac{\alpha_b}{\alpha_e}e\frac{C_c - \Gamma^*}{C_a} - \frac{\Gamma^*}{C_a}\frac{\alpha_b}{\alpha_f}f\right]. \quad (2)$$

Here, Δ^{13} is the modeled carbon isotope discrimination, t is a ternary correction factor dependent on the rate of transpiration and the conductance to CO_2 diffusion in air, R_d denotes the rate of mitochondrial respiration and Γ^* is the CO_2 compensation point in the absence of mitochondrial respiration. a_b, a_s, a_m, b, e, and f are the fractionations associated with diffusion through the laminar boundary layer, in air, in water (including the effect of dissolution), by Rubisco carboxylation, during respiration, and photorespiration, respectively, and $\alpha_b = 1+b$, $\alpha_e = 1+e$, and $\alpha_f = 1+f$ are the isotope effects of Rubisco carboxylation, respiration, and photorespiration. We have a fairly good idea of the values for a_b (2.9‰), a_s (4.4‰), and a_m (1.8‰). The fractionation b can be measured *in vitro* on extracted Rubisco and has been biochemically determined to be close to 29‰ with respect to gaseous CO_2 [24-26]. So far there is

no clear consensus on the value of f [27-31], associated with the fractionation of glycine decarboxylase, nor on the value of e, associated with the fractionation during mitochondrial respiration[11,32,33].

Because fractionation values are small, Eqn. (2) can be approximated by assuming $\alpha_b = \alpha_e = \alpha_f = 1$ without introducing a large error. Moreover, if measurements are done under low-moderate VPD we can set t=0 to get[34]:

$$\Delta^{13} = a_b \frac{C_a - C_s}{C_a} + a_s \frac{C_s - C_i}{C_a} + a_m \frac{C_i - C_c}{C_a} + b\frac{C_c}{C_a} - \frac{R_d}{A + R_d} e \frac{C_c - \Gamma^*}{C_a} - \frac{\Gamma^*}{C_a} f \quad (3)$$

Respiratory biochemistry and its treatment in the model

The treatment of respiration in the isotope discrimination model depends on two important considerations: The first one relates to whether the carbon compounds left behind by respiratory processes mix with the pool of respiratory substrate and by extension with the carbon in the Calvin-Benson-Bassham (CBB) cycle. In this case, the isotope effect of respiration is isotopically "connected" to the CBB cycle, and can thereby impose a change on the composition of the substrates of both respiration and photorespiration as there is effectively only one carbon pool (Fig. 1a). This is the assumption of the original model described above. The alternative case is that respiration is isotopically "disconnected" and metabolites are not fed back into the CBB cycle, which is equivalent to having two separate carbon pools: one that consists of compounds that are synthesized without involving a decarboxylation step, and one that is made up of compounds requiring a decarboxylation step, such as lipids and some amino acids (Fig. 1b). This, we argue, is likely the case. Respiratory CO_2 may be released from the TCA

cycle in the mitochondria during amino acid synthesis, from pyruvate dehydrogenase in the chloroplast in the production of acetyl-CoA for lipid synthesis, or by the pentose phosphate pathway generating precursors for nucleotides. In all cases, the residual compounds from these anabolic or catabolic respiratory processes occuring in the light are not readily converted back to respiratory carbohydrates. The carbon left behind therefore changes the composition of the assimilates via non-carbohydrate compounds, but it does not affect the composition of the respiratory carbon substrate *per se* (Fig. 1b). This subtle difference in assumptions has a profound effect on the predicted carbon isotope discrimination, which will become apparent in the following derivations.

The second consideration relates to the source of carbon used as substrate for respiration. This substrate carbon can be "recent", meaning it is impacted in the short-term by the isotope ratio of the CO_2 assimilated during the period of measurement, or it can be "old", i.e. the substrate has been assimilated at some point before the measurement is performed and therefore carries the isotopic signature of the CO_2 the plant was exposed to during growth. Differences in the manner of accounting for substrate that consists of old carbon also significantly impact the estimation of carbon isotope discrimination.

Derivation of the model

The schematic in Fig. 1c demonstrates the within-cell pathway of the carbon involved in photosynthesis and photorespiration. Carbon enters this pathway through the carboxylation of RuBP by Rubisco and can exit either via glycine decarboxylation (photorespiration) or as triose phosphates (TP; i.e. the assimilated carbon before respiration). Branch points in the pathway

where a net effect on the isotopic composition can occur are the carboxylation step by Rubisco and at glycine decarboxylation[35]. An additional branch point outlined in Fig. 1c that potentially fractionates is at the export step of triose phosphates from the CBB cycle, which we have included here for completeness and termed *h*. The parameter *h* can be viewed as an apparent fractionation factor resulting from starch formation, the kinetic fractionation associated with the export of triose phosphates from the chloroplast and the fractionation associated with enzymes such as aldolase, transaldolase, transketolase, and triose phosphate isomerase[36,37]. In contrast to the fractionations lumped into *e* that do not affect the composition of carbon in the CBB cycle, *h* as used here comprises isotopic effects that feed back into the CBB cycle. So far there is no information available on the magnitude of *h*. In addition to the fluxes, in terms of the rate of Rubisco carboxylation (V_c) and oxygenation (V_o), Fig. 1c also displays the average expected isotope ratio of the carbon in the metabolites involved in this pathway. For convenience, we assume that the isotope ratio is uniform within molecules. However, in reality there are positional effects on the intramolecular distribution of ^{13}C [36], which might influence, and even be responsible for, the values of both *h* and *e*.

We initially derive the isotope ratios of the CBB cycle metabolites in terms of the isotope ratio of ribulose 1,5-bisphosphate (RuBP; R_{RuBP}), the key metabolite in this pathway. Given a photorespiratory fractionation of *f*, the isotope ratio of the photorespired CO_2 is then described by $R_{\mathrm{RuBP}}/\alpha_{\mathrm{f}}$, leaving behind an isotope ratio of $\left(1+\frac{f}{3\alpha_{\mathrm{f}}}\right)R_{\mathrm{RuBP}}$ for serine and the 3-phosphoglycerate (PGA) derived from it (Fig. 1c, Supplementary Information, Section 2). The PGA that includes the newly assimilated carbon will have an average isotope ratio of

205 $\frac{1}{3}\left(2R_{\mathrm{RuBP}}+\frac{R_{\mathrm{Cc}}}{\alpha_{\mathrm{b}}}\right)$, reflecting the fact that two thirds of the carbon originate from the substrate

206 RuBP, while the remaining third consists of chloroplastic CO_2 (R_{Cc}) that has been discriminated

207 against by Rubisco during the carboxylation reaction. The second PGA stemming from the

208 carboxylation reaction and that derived from the oxygenation reaction will have the same

209 isotope ratio as RuBP, as no carbon is added or lost. We use mass balance considerations to

210 determine R_{PGA} by summing all incoming fluxes of PGA in terms of carbon (see Fig. 1c):

211 $$\left(6V_{\mathrm{c}}+\frac{9}{2}V_{\mathrm{o}}\right)R_{\mathrm{PGA}}=V_{\mathrm{c}}\left(2R_{\mathrm{RuBP}}+\frac{R_{\mathrm{Cc}}}{\alpha_{\mathrm{b}}}\right)+3\left(V_{\mathrm{c}}+V_{\mathrm{o}}\right)R_{\mathrm{RuBP}}+1.5V_{\mathrm{o}}\left(1+\frac{f}{3\alpha_{\mathrm{f}}}\right)R_{\mathrm{RuBP}}\,. \qquad (4)$$

212 If we assume a fractionation of *h* occurring during the export of TP from the CBB cycle,

213 then the isotope ratio of the exported TP (R_{TP}) is described in terms of that of PGA (R_{PGA}) by:

214 $$R_{\mathrm{TP}}=\frac{R_{\mathrm{PGA}}}{\alpha_{\mathrm{h}}}\,, \qquad (5)$$

215 where $\alpha_{\mathrm{h}}=1+h$.

216 We calculate R_{RuBP} as a function of R_{PGA} by considering RuBP as the product of the

217 CBB cycle that incorporates the fractionation involved with TP utilization. This yields

218 $$\left(V_{\mathrm{c}}-0.5V_{\mathrm{o}}\right)\frac{R_{\mathrm{PGA}}}{\alpha_{\mathrm{h}}}+5\left(V_{\mathrm{c}}+V_{\mathrm{o}}\right)R_{\mathrm{RuBP}}=\left(6V_{\mathrm{c}}+\frac{9}{2}V_{\mathrm{o}}\right)R_{\mathrm{PGA}}\,, \qquad (6)$$

219 which can be solved for R_{RuBP} as:

220 $$R_{\mathrm{RuBP}}=\frac{1+wh}{\alpha_{\mathrm{h}}}R_{\mathrm{PGA}}\,, \qquad (7)$$

where we set $w = \frac{6C_c + 9\Gamma^*}{5C_c + 10\Gamma^*}$ for convenience. The details of the derivations are outlined in the Supplementary Information, Section 2.

Substituting R_{RuBP} from Eqn. (4) for that in Eqn. (7) and then rearranging, results in an expression for R_{PGA} (see Supplementary Information, Section 3):

$$R_{PGA} = \frac{\alpha_h}{\alpha_b} \frac{R_{Cc}}{1 - \frac{\Gamma^*}{C_c} \frac{(f - wh)}{\alpha_f}} \quad (8)$$

Substituting Eqn. (8) in Eqn. (5) then determines R_{TP} in terms of R_{Cc}:

$$R_{TP} = \frac{R_{Cc}}{\alpha_b} \frac{1}{1 - \frac{\Gamma^*}{C_c} \frac{(f - wh)}{\alpha_f}} \quad (9)$$

To determine R_A we employ mass balance considerations and obtain from the carbon isotope ratios of TP and respired CO_2 (Fig. 1c):

$$(V_c - 0.5V_o)R_{TP} = (A + R_d)R_{TP} = AR_A + R_d \frac{R_{TP}}{\alpha_e} \quad (10)$$

which can be solved for R_A as

$$R_A = R_{TP}\left(1 + \frac{R_d}{A}\frac{e}{\alpha_e}\right) \quad (11)$$

We then combine Eqns. (9) and (11) to relate R_{Cc} to R_A:

$$R_{Cc} = \frac{R_A}{\alpha_R}\left(\alpha_b - \frac{\alpha_b}{\alpha_f}\frac{\Gamma^*}{C_c}(f - wh)\right), \quad (12)$$

where for convenience we set $\alpha_R = 1 + \frac{R_d}{A}\frac{e}{\alpha_e}$. R_{Cc} can now be related to R_{Ca}, the isotope ratio of the CO_2 in the ambient air[23] (see Supplementary Information, Section 4). By definition,

the carbon isotope discrimination of a plant is related to the isotope ratios of the CO_2 in ambient air and that of the assimilates by $\alpha^{13} = 1 + \Delta^{13} = R_{Ca} / R_A$, from which our new equation of the carbon isotope discrimination of a leaf including ternary effects is calculated as:

$$\Delta^{13} = \frac{1}{1-t}\left[a_b \frac{C_a - C_s}{C_a} + a_s \frac{C_s - C_i}{C_a}\right] + \frac{1+t}{1-t}\left[a_m \frac{C_i - C_c}{C_a} + b\frac{C_c}{C_a} - \frac{R_d}{A}\frac{\alpha_b}{\alpha_e \alpha_R} e \frac{C_c}{C_a} - \frac{\alpha_b}{\alpha_f \alpha_R}\frac{\Gamma^*}{C_a}\left(f - wh\right)\right] \quad (13)$$

The full derivation including *h* will be useful for interpreting *f* and may have practical importance should more information about the nature of *h* become available in the future. However, to facilitate an easy comparison with the old model it is helpful to assume that *h* = 0 and drop the *h*-term for the moment. Using the same simplifying assumptions as for Eqn. (3) we can write Eqn. (13) as

$$\Delta^{13} = a_b \frac{C_a - C_s}{C_a} + a_s \frac{C_s - C_i}{C_a} + a_m \frac{C_i - C_c}{C_a} + b\frac{C_c}{C_a} - \frac{R_d}{A} e \frac{C_c}{C_a} - \frac{\Gamma^*}{C_a} f \ . \quad (14)$$

This simplified equation is similar, although not equivalent, to one developed previously[11] to include the effects of root and stem respiration in a mesocosm study. That model has R_d in ratio to *A*, as in Eqn. (14), but because it assumes that all the respiration is released into the ambient air, it does not weight respiration by C_c / C_a. The latter ratio is needed for a leaf model to account for the fact that not all of the respiratory isotope effect is expressed due to the refixation of respired CO_2 inside the leaf, which becomes important e.g. under water stress conditions when C_c / C_a is small.

Comparing Eqn. (14) with Eqn. (3) then shows that the only difference between the two equations is related to the term for respiratory discrimination. In contrast to Eqn. (3), which

effectively scales R_d relative to the flux V_c (note that $\frac{R_d}{A+R_d}\frac{C_c-\Gamma^*}{C_a}=\frac{R_d}{V_c}\frac{C_c}{C_a}$ Ref. [38]), Eqn. (14) scales R_d with A. While the difference between the two formulations is small under conditions where R_d is small compared to A, it may become quite large when A approaches zero. To fully assess the impact of this modification in the isotope discrimination model we compare the two models without any simplifications from here on.

Isotope discrimination in the two-resistance case

The models described above implicitly assume that in effect all (photo)respired CO_2 is released inside the chloroplast. As pointed out previously, if all or some respired or photorespired CO_2 mixes with the CO_2 coming in from the intercellular space inside the cytosol (with the CO_2 concentration denoted C_m), one has to treat the diffusive resistance for CO_2 across the cell wall separately from the resistance between the cytosol and the inside of the chloroplast[10,39,40]. This causes g_m to apparently vary with environmental conditions, even when the individual resistances are fixed[39]. Notably, the apparent g_m is expected to become zero at the compensation point, following the relation[10,41]

$$g_m=\left[r_{wp}+r_{ch}\left(1+\gamma\frac{F+R_d}{A}\right)\right]^{-1} \quad (15)$$

where r_{wp} represents the resistance across the cell wall and plasmalemma, r_{ch} the resistance of the chloroplast envelope and stroma, and γ is the fraction of (photo)respired CO_2 that diffuses into the cytosol. Note that γ can be very small, yet still cause g_m to decline as A approaches zero. The effect of this two-resistance diffusion model on carbon isotope discrimination has

been described before[10,27] using the assumptions for respiration made by Farquhar, et al. [8]. Here, we give an updated version of the two-resistance isotope discrimination model accounting for both respiration using old substrate and not feeding back into the CBB cycle. For simplicity we set $\gamma = 1$, representing the extreme case where all released CO_2 first diffuses into the cytosol, as originally proposed by Tholen, et al. [39]. Then isotope discrimination can be described by (see Supplementary Information, Section 5 for the derivation):

$$\Delta^{13} = \frac{1}{1-t}\left[a_b\frac{C_a - C_s}{C_a} + a_s\frac{C_s - C_i}{C_a}\right] + \frac{1+t}{1-t}\left[\begin{array}{l} a_m\frac{C_i - C_m}{C_a} + a_c\frac{C_m - C_c}{C_a} + b\frac{C_c}{C_a} \\ -\frac{R_d}{A}\frac{\alpha_c}{\alpha_e\alpha_R}e\left(\frac{C_m}{C_a} + \frac{b-a_c}{\alpha_c}\frac{C_c}{C_a}\right) - \frac{\alpha_c}{\alpha_f\alpha_R}\frac{\Gamma^*}{C_c}\left(f - wh\right)\left(\frac{C_m}{C_a} + \frac{b-a_c}{\alpha_c}\frac{C_c}{C_a}\right) \end{array}\right] \quad (16)$$

where a_c is the fractionation associated with CO_2 diffusion from the cytosol to the site of carboxylation and $\alpha_c = 1 + a_c$. For the case of $0 < \gamma < 1$ isotope discrimination is expected to be intermediate to that predicted by Eqns. (13) and (16).

Respiratory fractionation *e*

As with the fractionation *h*, *e* as used here is not determined by a single enzymatic reaction. Rather it is defined by the difference in the isotopic ratio of the carbon assimilated and the released CO_2, which is coming from multiple sources[42]. The fractionation *e* therefore is a composite of the fractionations of the decarboxylating enzymes involved, but also includes the sum of all fractionations contributing to any difference in isotope ratio of the respiratory substrates relative to that of the primary assimilates R_{TP}. The latter includes potential

fractionation during carbon export from the chloroplast and the leaf, as well as during the allocation of carbon to different metabolic pathways[33,37].

Because photorespiration is dependent on the presence of light, one can safely assume that the substrate for photorespiration consists of freshly assimilated carbon. In contrast, the bulk of day respiration likely comes from substrates that are older[43-47]. This is especially the case when *A* is small during the measurement and therefore the rate of current substrate synthesis is low. If the isotope ratio of the CO_2 that is being assimilated during the measurement (R_A) is different from the isotope ratio of the respiratory substrate ($R_{substrate}$), the respiratory fractionation *e* needs to be adjusted by adding an apparent fractionation *e** taking into account this difference in substrate composition[46]. Wingate, et al. [46] proposed to replace *e* in the model with $e' = e + e^*$, where $e^* = R_A / R_{substrate} - 1$, which was applied as

$$\begin{aligned} e^* &= \delta_A^{meas} - \delta_{substrate} \\ &\approx \delta_{Ca}^{meas} - \Delta_{obs}^{meas} - \delta_{substrate} \end{aligned} . \quad (17)$$

Here Δ_{obs}^{meas} is the isotope discrimination and δ_A^{meas} the isotopic composition (δ; defined as the difference of the isotope ratio of a sample from that of a standard: $\delta = R_{sample} / R_{standard} - 1$) of the CO_2 assimilated during the measurement and $\delta_{substrate}$ that of the respiratory substrate. The conversion of Δ to δ is given by definition, and the carbon isotope discrimination of a plant is approximated by the difference of the composition of the air and the carbon that is assimilated[4]:

$$\begin{aligned} \Delta_{obs}^{13} &= \frac{\delta_{Ca} - \delta_A}{1 + \delta_A} \\ &\approx \delta_{Ca} - \delta_A \end{aligned} \quad (18)$$

$\delta_{substrate}$ has previously been taken as the isotopic composition of CO_2 respired in the dark[46]. Strictly, however, this approach needs to include the effect of respiratory fractionation in determining $\delta_{substrate}$, which also assumes that we have good knowledge of the value of *e* in the first place. In addition, *e* would have to be constant, independent of the environmental condition to which the plant is exposed and, most importantly, would need to be the same in the dark and the light. This, however, is uncertain given the multiple sources of respired CO_2 [33]. Because $\delta_{substrate}$ is usually not known, it is a common practice to simplify Eqn. (17) to

$$e^* = \delta_{Ca}^{meas} - \delta_{Ca}^{growth} \tag{19}$$

or $e^* = \delta_{CO2tank} - \delta_{Ca}^{growth}$ (see e.g. [14,27,48-52]), where δ_{Ca}^{growth} is the isotopic composition of ambient air during growth (approximately -8‰ in the natural environment) and $\delta_{CO2tank}$ is the isotopic composition of the CO_2 used for the measurement. This simplification is problematic, since Δ_{obs} changes substantially with the isotopic composition of the measurement gas. As we will see, even when measured with a gas that has a composition close to that of ambient air, Δ_{obs} changes with environmental factors, such as light intensity. Instead, we propose to calculate *e** as the difference in the isotopic composition of recent and old assimilates, which should give a good approximation of the difference in the composition of recent to old respiratory substrate assuming that the general biochemistry of the leaf stays constant. Knowledge of $\delta_{substrate}$ *per se* is therefore not required. This gives

$$\begin{aligned} e^* &= \delta_{substrate}^{meas} - \delta_{substrate}^{growth} \\ &\approx \delta_{A}^{meas} - \delta_{A}^{growth} \\ &\approx \left(\delta_{Ca}^{meas} - \Delta_{obs}^{meas}\right) - \left(\delta_{Ca}^{growth} - \Delta_{obs}^{growth}\right) \end{aligned} \tag{20}$$

using Eqn. (18) and where the superscript 'growth' denotes isotope composition and discrimination during the time the respiratory substrate was assimilated. Here, we use the observed discrimination against ^{13}C, measured under ambient growth conditions, for Δ_{obs}^{growth}. This approach does not require prior knowledge of *e*, and it avoids the issue that there may be further fractionations occurring between the assimilated carbon and the actual substrate for respiration. Uncertainties in the values of δ_{Ca}^{growth}, Δ_{obs}^{growth}, or *e* will equally affect the absolute value of *e*' as a constant offset, equal for any value of $\delta_{CO2tank}$ used, allowing us to compare measurements made with different $\delta_{CO2tank}$.

Calculation of g_m from carbon isotope measurements

Most commonly, isotope discrimination models are used to estimate C_c for the calculation of g_m, assuming that all other parameters such as fractionation values are known or can be measured independently. We can derive g_m from the old model that assumes R_d to be isotopically connected to the CBB cycle (g_m^{con}) by calculating $\Delta_i - \Delta_{obs}^{13}$, where Δ_i is defined by Eqn. (2) with g_m assumed to be infinite, i.e. when $C_c = C_i$, and Δ_{obs}^{13} is the observed discrimination. Substituting $C_i - C_c = A/g_m$ and solving for g_m we obtain[9,23]:

$$g_m^{con} = \frac{1+t}{1-t} \frac{A\left(b - a_m - \frac{R_d}{A+R_d}\frac{\alpha_b}{\alpha_e}e'\right)}{C_a\left(\Delta_i - \Delta_{obs}^{13}\right)} \quad . \tag{21}$$

Analogously, we solve Eqn. (13) for g_m derived from the new model assuming R_d is isotopically disconnected from the CBB cycle (g_m^{dis}) as:

$$g_{\mathrm{m}}^{\mathrm{dis}} = \frac{1+t}{1-t}\frac{A\left(b - a_{\mathrm{m}} - \frac{R_{\mathrm{d}}}{A}\frac{\alpha_{\mathrm{b}}}{\alpha_{\mathrm{e}}\alpha_{\mathrm{R}}}e'\right)}{C_{\mathrm{a}}\left(\Delta_{\mathrm{i}} - \Delta_{\mathrm{obs}}^{13}\right)}\,, \tag{22}$$

which is valid when $h = 0$ and a very close approximation of $g_{\mathrm{m}}^{\mathrm{dis}}$ when $h \neq 0$ (for derivation see Supplementary Information, Section 6).

Because there is no simple analytical solution to Eqn. (16) we have numerically solved for g_{m} by modeling Δ^{13} with a given value of C_{c} and then varying C_{c} to minimize the sum of squares between the modeled Δ^{13} and the observed discrimination $\Delta_{\mathrm{obs}}^{13}$. We can then calculate the apparent g_{m} from C_{c} as $g_{\mathrm{m}} = \frac{A}{C_{\mathrm{i}} - C_{\mathrm{c}}}$.

Assessing the sources contributing to Δ^{13}

Using the notation of Ubierna and Farquhar [34] we can write Eqn. (2) as:

$$\Delta^{13} = \Delta_{\mathrm{b}} - \Delta_{\mathrm{gb+gs}} - \Delta_{\mathrm{gm}} - \Delta_{\mathrm{e'}} - \Delta_{\mathrm{f}}\,, \tag{23}$$

where Δ_{b}, $\Delta_{\mathrm{gb+gs}}$, Δ_{gm}, $\Delta_{\mathrm{e'}}$, and Δ_{f} are the discriminations associated with Rubisco, diffusion through the boundary layer and stomata, through the mesophyll, respiration, and photorespiration, respectively. The individual components for when R_{d} is isotopically connected to the CBB cycle (superscript 'con') can be calculated as[34]:

$$\Delta_{\mathrm{b}}^{\mathrm{con}} = \frac{1+t}{1-t}b \tag{24}$$

$$\Delta_{\mathrm{gb+gs}}^{\mathrm{con}} = \frac{1+t}{1-t}\left[\left(b - \frac{\bar{a}}{1+t}\right)\frac{C_{\mathrm{a}} - C_{\mathrm{i}}}{C_{\mathrm{a}}}\right] \tag{25}$$

$$\Delta_{gm}^{con} = \frac{1+t}{1-t}\left[\left(b - a_m\right)\frac{C_i - C_c}{C_a}\right] \quad (26)$$

$$\Delta_{e'}^{con} = \frac{1+t}{1-t}\left[\frac{R_d}{A+R_d}\frac{\alpha_b}{\alpha_e}e'\frac{C_c - \Gamma^*}{C_a}\right] \quad (27)$$

$$\Delta_{f}^{con} = \frac{1+t}{1-t}\left[\frac{\alpha_b}{\alpha_f}\frac{\Gamma^*}{C_a}f\right], \quad (28)$$

where we define $\bar{a} = \frac{a_b\left(C_a - C_s\right) + a_s\left(C_s - C_i\right)}{C_a - C_i}$ as the weighted fractionation across the boundary layer and stomata in series. The discrimination model developed here assuming R_d to be isotopically disconnected (Eqn. (13)) can be split in a similar way (superscript 'dis'). The equations for Δ_b^{dis}, Δ_{gb+gs}^{dis} and Δ_{gm}^{dis} are identical to their respective components of the old model, although they do not necessarily attain the same value due to a difference in estimated C_c. In the new model $\Delta_{e'}^{con}$ and Δ_f^{con} are replaced by

$$\Delta_{e'}^{dis} = \frac{1+t}{1-t}\left[\frac{R_d}{A}\frac{\alpha_b}{\alpha_{e'}\alpha_R}e'\frac{C_c}{C_a}\right] \quad (29)$$

and

$$\Delta_{f\text{-}wh}^{dis} = \frac{1+t}{1-t}\left[\frac{\alpha_b}{\alpha_f\alpha_R}\frac{\Gamma^*}{C_a}\left(f - wh\right)\right], \quad (30)$$

respectively.

Experimental testing of the model

383 The calculation of g_m from gas exchange and carbon isotope measurements depends on Δ_{obs}^{13}
384 (see e.g. Eqn. (21)), but should not be affected by δ_{Ca} for any given set of fractionation factors.
385 If calculated g_m values were to change with δ_{Ca} this would indicate that the model in use does
386 not account for respiration appropriately, since the respiration contribution is the only term
387 currently in the discrimination model that has δ_{Ca} as an input. We can make use of this feature
388 to compare the models described above that differ in how they treat respiration (isotopically
389 connected vs. disconnected) and in the way *e** accounts for old respiratory substrate. In the
390 following we present results using data obtained with source CO_2 of two different isotopic
391 compositions, one close to ambient air ($\delta_{CO2tank} = -7.0‰$) and one depleted in ^{13}C (
392 $\delta_{CO2tank} = -30.7‰$).

393 Figure 2 shows the CO_2 responses of g_m calculated from the original isotope
394 discrimination model assuming R_d is isotopically connected (Eqn. (2)) and the model derived
395 here assuming R_d is isotopically disconnected (Eqn. (13)), both with the commonly used
396 simplification of *e** (Eqn. (19)), or its calculation according to Eqn. (20) taking into account that
397 Δ_{obs} changes with the environment. Only for the discrimination model derived here in
398 combination with accounting of *e** based on δ_A do the g_m values agree with each other when
399 measured with different $\delta_{CO2tank}$ (Fig. 2d). In all other cases, differences in g_m due to $\delta_{CO2tank}$
400 increase under conditions where R_d is large relative to *A*, and g_m values frequently become
401 negative, which renders them biologically meaningless given that *A* is positive. In other words,
402 g_m values are reasonable at any measured CO_2 concentration if we treat respiration as
403 isotopically disconnected from the CBB cycle (related to the new parameterization of

404 respiration in the discrimination model) and assume that the difference in composition
405 between old and new respiratory substrate is approximated by the difference in composition
406 between old and new assimilates (related to the parameterization of *e**).

407 Figure 3 compares the discriminations associated with Rubisco (Δ_b), diffusion through
408 the boundary layer and stomata (Δ_{gb+gs}), through the mesophyll (Δ_{gm}), respiration ($\Delta_{e'}$), and
409 photorespiration (Δ_f) between the original 'connected' and the new 'disconnected' model,
410 accounting for *e** according to Eqn. (20) and assuming *h*=0. While the model used has hardly
411 any effect on Δ_b and Δ_{gb+gs} (Fig. 3a-b, f-g) and only minor effects on Δ_f (Fig. 3e, j), the
412 differences in $\Delta_{e'}$ are marked and the disconnected model shows discriminations at low CO_2
413 concentrations that are more than twice those of the connected model (Fig. 3d, i). The residual
414 discrimination that is not explained by Δ_b, Δ_{gb+gs}, $\Delta_{e'}$, and Δ_f is attributed to Δ_{gm}. The two
415 gases with differing values of $\delta_{CO2tank}$ result in similar Δ_{gm} values in the disconnected model,
416 while they progressively further deviate towards low C_i using the connected model (Fig. 3c, h).
417 Negative Δ_{gm} values with the connected model correspond to unrealistic negative g_m values.

418 CO_2 and light response curves of photosynthetic and isotope parameters are shown in
419 Figure 4. Values of *A* (Fig. 4a-c; only values for $\delta_{CO2tank} = -7.0‰$ are shown as they are virtually
420 indistiguishable from values measured with $\delta_{CO2tank} = -30.7‰$) were measured down towards
421 the compensation point, where *A* is small compared to R_d, i.e. at low C_i or low light intensity.
422 Corresponding values of Δ^{13}_{obs} increasingly deviate with decreasing C_i for the two gases used
423 (Fig. 4d-f). Derived values of *e** strongly depend on the way *e** is calculated (Fig. 4g-l). While

424 generally larger differences between the two calculations are observed in measurements made
425 at $\delta_{CO2tank} = -30.7‰$ (exceeding 50‰ at low C_i; Fig. 4j-l), e^* is far from constant even at
426 measurements made with a CO_2 composition close to that of ambient air ($\delta_{CO2tank} = -7.0‰$;
427 Fig. 4g-h). This impacts the g_m estimates obtained with the different carbon isotope
428 discrimination models. Figure 5 shows how g_m differs when estimated with the four different
429 model assumptions outlined in Figure 2. The behavior of the g_m estimate is highly dependent
430 on $\delta_{CO2tank}$ for all model assumptions except for the new discrimination model when using Eqn.
431 (20) for e^* (Fig. 5). This model achieves positive g_m values under any condition of the CO_2
432 responses at 21% and 2% O_2 as well as the light response curves, and the values match for both
433 gases used.

434 The photorespiratory fractionation f has the most uncertain value of all fractionations
435 used by the models. While the theoretical value of f is 11‰ [53], experimental values have been
436 reported *in vivo* ranging from 7 to 16‰ [27,29-31], and estimates reported from *in vitro* assays even
437 include negative values[54,55]. Estimates of g_m are also highly sensitive to f, making this parameter
438 important for many applications of discrimination models. Figure 6 explores the impact of f on
439 the calculated g_m. Independent of f, the old model (Eqn. (2)) predicts different values of g_m
440 depending on $\delta_{CO2tank}$ (Fig. 6a-d). In contrast, predictions of g_m with both gases used gave
441 similar values independent of f using the new model. Similar trends are observed when the
442 value of e is varied (Fig. S1). While the absolute values of g_m vary with e and f, the chosen
443 values have a negligible impact on the overall shape of the CO_2 response of g_m estimated with

444 the new model, with g_m decreasing to zero as the compensation point is approached (Figs. 6e-h
445 and S1).

446 Because a decrease of g_m towards the compensation point is in support of a two-
447 resistance situation for CO_2 diffusion in the mesophyll, we investigated whether the
448 assumptions in the discrimination model regarding diffusion resistances affect the estimated
449 apparent g_m. Figure 7 compares g_m calculated assuming a single mesophyll resistance (following
450 Eqn. (13)) with the apparent g_m calculated with a two-resistance discrimination model
451 (following Eqn. (16)). Both CO_2 and light responses return similar values of g_m for the two
452 isotope discrimination models used.

453

454 **Assumptions regarding respiration impact model outcomes**

455 The original model of carbon isotope discrimination by Farquhar, et al. [8] was built on the
456 assumption that respiration uses recent assimilates as substrate and that the carbon
457 compounds left behind after respiration can mix with those in the CBB cycle. However, much of
458 the respiratory substrate appears to have been assimilated at a time long before a typical
459 measurement is taken[43-47] and the decarboxylation reactions linked to anabolic processes in the
460 light produce organic compounds that are not easily converted back to TP[33,37]. Both effects
461 make it unlikely that respiration instantaneously feeds back into carbon skeletons of the CBB
462 cycle. While the use of 'old' respiratory substrate excludes a full isotopic connectivity between
463 ongoing photosynthesis and respiration by definition, the connectivity is also broken in the case
464 of respiration drawing from all newly synthesized carbon because of the missing feedback from
465 respiratory products, such as lipids and amino acids, to the CBB cycle.

Taking this more realistic treatment of respiration into account, our new derivation has a fundamental impact on the predictions obtained from the model. Differences between the models become particularly obvious under conditions where R_d becomes large relative to A. Indeed, the odd predictions for g_m under these conditions illustrated here and elsewhere are what prompted us to re-evaluate the theory behind the existing model. Using two sources of CO_2 with different values of $\delta_{CO2tank}$ [3,56] enables testing of the quality of the model independent of the more uncertain fractionation values, such as e and f (Fig. 2). While the absolute values of the estimated g_m will change with the values of e and f, estimates should be the same independent of $\delta_{CO2tank}$. We found that this was not the case when respiration was assumed to be isotopically connected to the CBB cycle, or when the calculation of e^* ignored the variability of Δ_{obs}^{13}. The agreement between g_m estimates obtained with a wide range of values of f provides evidence that the 'disconnected' model is much more robust (Fig. 6). Further research can build on this knowledge to gain a better understanding of the fractionation values, since their quantifications often rely on the use of the discrimination model itself.

Is there a need in the model to consider *h*?

At the moment we do not have a clear picture of the nature of h, or a detailed understanding of the processes contributing to this fractionation occurring during TP export from the CBB cycle, which makes it difficult to assign a value to h. Parameterizing h in the model is instructive, however, for gaining a deeper insight into the variability of f. As can be seen from Eqn. (13), both f and h scale with Γ^*/C_a and behave as a combined fractionation with magnitude

$\left(f - wh\right)$. Not accounting for *h* in the model implicitly attributes any effect of *h* to the photorespiratory fractionation, resulting in an apparent value of *f* that is roughly equivalent to the difference between *f* and *h*. While *f* may be well-defined by the single process of glycine decarboxylation, *h* can be viewed as a lumped factor made up of different enzymatic reactions and diffusion/transport processes. A fractionation by any of these factors will likely result in variability of *h* related to changes in the relative magnitude of these factors, determined by the rate and fate of triose-phosphates exported from the CBB cycle at any given time. We therefore expect *h* to vary with plant species due to the differences in their biochemistry, the plant's growth conditions and the environmental conditions during the measurement. The confounding effect of *h* on *f* may explain in part the large variability of reported values of *f* measured *in vivo*.

On the importance of including *e**

It has long been known that because plants mostly respire previously assimilated substrate one needs to account for the difference in isotopic composition between the respired and assimilated CO_2. Several approaches of accounting for this effect are in use[14,46,48], but proper testing of their suitability has been complicated by the issues related to the respiratory discrimination component of the original discrimination model, outlined in this report. Based on comparing g_m estimates obtained from two $\delta_{CO2tank}$ source tanks, calculated using the two different discrimination models, we conclude that defining *e** as in Eqn. (20) best accounts for the differences in isotopic composition between assimilated and respired CO_2. While the respiratory substrate might not be entirely old carbon under all conditions, it is likely the case

when A is close to zero, which is where the impact of respiration is most pronounced. Small proportions of unaccounted-for new carbon under large A will have a negligible effect on the estimated g_m, as R_d/A will be small.

It is important not to simplify e^* as is done in Eqn. (19), because Δ_{obs}^{13} changes substantially with the measurement condition (Fig. 4). Since this is the case even when using a measurement gas that has an isotopic composition similar to that of ambient air, the inclusion of e^* is strictly necessary when measuring close to the CO_2 or light compensation points (Figs. 4 and 5). We further demonstrate that a proper accounting of e^* is only satisfactory in combination with the model derived here (Fig. 2).

More robust estimation of g_m

The comparison of g_m calculated with the different models demonstrates that only the new model derived here in combination with e^* as defined in Eqn. (20) returns positive g_m values for all CO_2 concentrations and both source CO_2 isotopic compositions (Fig. 2) and for a large range of potential values of e and f (Figs. 6 and S1). Similarly, it constitutes the most consistent treatment for the calculation of g_m in response to CO_2 at low O_2 concentrations as well as to a wide range of light intensities (Fig. 5). A major point of controversy in recent years has been whether or not g_m decreases towards zero at the CO_2 compensation point, which can be taken as evidence for or against a multi-resistance pathway for CO_2 diffusion in the mesophyll. A decrease towards zero is what would be expected if some proportion of (photo)respired CO_2 is mixing in the cytosol with the CO_2 coming in from the IAS, indicating that the diffusive resistance across the cell wall has to be treated separately from the resistance across the

chloroplast membrane[10,39]. With the old model this was difficult to assess, as the shape of the CO_2 response of g_m strongly depended on the fractionation values used, and, ignoring the values at very low [CO_2] that often became unrealistically negative, may indicate a decrease of g_m towards the compensation point (for $f \leq 7‰$; Fig. 6a,b,d), a g_m constant with changing [CO_2] (for $f \approx 10‰$), or g_m increasing with decreasing [CO_2] ($f \geq 11‰$; Fig. 2, Fig. 6c). While the absolute values of g_m derived with the new model still depend on the values of *e* and *f* (and *h* if applicable), the overall shape of the CO_2-response, and in particular the decrease of g_m to zero around the compensation point, is common to a wide range of possible fractionation values (Fig. 6e-h). These results obtained from carbon isotopes now agree with many of the values derived from chlorophyll fluorescence[15,16]. While there may be other causes of g_m changing with CO_2 concentration, g_m decreases to zero precisely when approaching the compensation point, which would be a peculiar coincidence if not for two mesophyll resistances. From this we can more confidently conclude that a single-resistance view of mesophyll conductance is too simplistic and a more complex multiple-resistance model of photosynthesis should be considered[10,39,40].

Based on the data presented here, however, there may be no urgent need to apply a more complicated two-resistance isotope discrimination model. Apparent values of g_m estimated with the two-resistance model are similar to those derived with the single-resistance model, which can be explained by the models differing only by the fractionation created from CO_2 diffusion in liquid from the cytosol to the chloroplast. This agreement in g_m responses highlights the fact that our g_m estimates using carbon isotopes are largely independent of our assumptions regarding CO_2 diffusion inside the mesophyll. One consequence of this result is

553 that values of f determined with the assumption that g_m is insensitive to changes in the O_2
554 concentration (i.e. requiring the single-resistance case)[27,30] have to be treated with care.
555 Further work is required to quantitatively separate the apparent mesophyll resistance
556 into r_{wp} and r_{ch}. Only then can we assess how much of the variability of g_m observed with
557 changing environmental conditions can be explained by a two-resistance scenario alone.
558
559 **Conclusion**
560 The isotope discrimination model presented here proved experimentally to be more robust
561 than the old model, in particular under conditions where R_d/A is large. Our results suggest that
562 the new formulation of the respiratory term results in more accurate estimations of g_m under a
563 wide range of conditions, allowing us to more confidently interpret mesophyll diffusion
564 properties. The new model will also improve our understanding of plant responses to drought
565 and estimations of water-use efficiency derived from the isotopic composition of leaf dry
566 matter, as the differences from the old model are most pronounced under the low C_i values
567 seen when stomata are relatively closed. This may ultimately help to uncover new strategies to
568 improve water-use efficiency of crop plants in water-limited environments. Given its more
569 mechanistic implementation of respiration we expect the new model not only to perform
570 better with leaf-level online isotope discrimination approaches, but to provide improved
571 accuracy on the carbon exchange of plants at any level, which is imperative for correct
572 modelling of the global carbon cycle.
573
574

Methods

Plant Material

Wheat (*Triticum aestivum* L. cv 'Sunstate') plants were grown in controlled glasshouse conditions (25°C day/17°C night) under natural light. Seeds were germinated and grown in 5L pots filled with Martins Potting Mix (Martins Fertilizers, Yass, NSW, Australia) and an initial addition of 5g of slow-release Osmocote fertilizer (Scotts Australia, Bella Vista, NSW, Australia). Plants were watered daily and received an additional dose of liquid fertilizer once they were established. Gas exchange and online carbon isotope discrimination were measured on fully expanded flag leaves of eight- to ten-week-old plants.

Gas exchange and isotopic measurements

An LI-6400XT open gas exchange system (Li-Cor, Lincoln, NE, USA) was coupled to a dual quantum cascade laser (QCL) absorption spectrometer (Aerodyne Research Inc, Billerica, MA, USA), which measured isotopologues of CO_2 including $^{12}CO_2$ and $^{13}CO_2$ (described in detail by Holloway-Phillips, et al. [56]). The LI-6400XT was assembled with the 6400-07 needle chamber (12 cm^2) fitted with an LI-6400-18 RGB light source set to a red-blue ratio of 90:10. Gas was sampled from the inlet gas line to the leaf cuvette ("reference gas") or the outflow of the cuvette ("sample gas") and subsequently dried by a Nafion (The Chemours Company, Wilmington, DE, USA) dryer and dry-ice trap. Synthetic air was mixed from O_2 and N_2 using two mass flow controllers to achieve the 21% or 2% [O_2] used in the experiments. Part of this mix flowed through a temperature-controlled bubbling flask for humidification, which provided the

gas for the LI-6400XT. The other part was mixed with gas carrying CO_2 of known concentration and isotopic composition ("calibration gas"). The selected high-pressure CO_2 tank supplied both the calibration gas and the LI-6400XT console, so that when the CO_2 source gas for the cuvette was switched, the data could be corrected to its true δ^{13} value using the calibration gas of the same isotopic composition[56]. Two concentrations of the calibration gas spanning the chamber reference and sample gas concentrations were measured at the beginning and end of each measurement cycle, which included three alternating reference/sample pairs. This calibration accounted for both the concentration dependence of the measured isotopic composition of CO_2 and drift of the machine between each measurement series. The observed composition values of the calibration gas could be treated as linear within the concentration ranges of the sample and reference concentrations. This allowed us to linearly interpolate between the observed compositions of the known calibration gas at two concentrations to calculate a δ_{offset} applied to the measured raw δ^{13} values of the sample and reference measurements. All δ^{13} values were expressed relative to the Vienna Pee Dee Belemnite standard with an isotope ratio of $R_{\text{VPDB(carbon)}} = 0.0111797$ as $\delta^{13} = \left({}^{13}\text{CO}_2 / {}^{12}\text{CO}_2\right) / R_{\text{VPDB(carbon)}} - 1$.

To investigate the [CO_2] dependence of g_m, gas exchange and isotopic fluxes were measured on flag leaves of three to five distinct plants at 400, 250, 150, 100, 80 and 65 µmol mol^{-1} for measurements at 21% [O_2], and at 400, 250, 150, 100, 70 and 40 µmol mol^{-1} for measurements at 2% [O_2]. The measurement light intensity was set to 1400 µmol photons m^{-2} s^{-1}. For the light response of g_m, measurements were made at a CO_2 concentration surrounding the leaf of 400 µmol mol^{-1} and light intensities of 50, 100, 200, 400, 800 and 1400 µmol photons

618 m^{-2} s^{-1}. In all experiments leaf temperature was controlled at 30°C and VPD at 1kPa. Plants were
619 acclimated to each environmental condition for at least half an hour with one of the CO_2 source
620 gases before a measurement was taken. The apparatus was then switched to a second source
621 gas with different carbon isotope composition and a measurement was taken when δ_{Ca} in the
622 leaf cuvette was stable, which usually took less than 30 minutes. The isotopic compositions of
623 the two source gases used were $\delta_{CO2tank} = -7.0‰$ and $\delta_{CO2tank} = -30.7‰$.

624 For estimates of Δ_{obs}^{growth} plants were measured at a light intensity of 1400 µmol photons
625 m^{-2} s^{-1} and a CO_2 concentration of 400 µmol mol^{-1}. The common methods to measure R_d in the
626 light (Kok, Laisk, and isotopic disequilibrium methods)[3,57] depend on knowledge of diffusion
627 properties inside the leaf and can therefore not be used to determine R_d in the light
628 independently of g_m. However, it was previously shown that diffusion resistances inside the leaf
629 can explain much of the differences in observed rates of respiration in the light and the dark[57].
630 We have therefore assumed that R_d in the dark is the same as in the light and measured R_d in
631 the dark at the beginning of the day of the measurement. Inaccuracies in the value of R_d used
632 will affect the curvature of the measured g_m response curves, but not the decrease of g_m
633 towards zero as A approaches the compensation point. R_d as used here is defined as the sum of
634 all non-photorespiratory decarboxylations. Because detailed information about the origin of
635 individual respiratory fluxes is not available, we assumed that R_d originates exclusively in the
636 chloroplast (single-resistance model) or the mitochondria (two-resistance model). However,
637 non-photorespiratory decarboxylations may simultaneously occur in mitochondria, chloroplasts
638 and cytosol. In this case a situation intermediate between the single-resistance and the two-
639 resistance model is to be expected.

640

641 **Estimating resistances with the two-resistance model**

642 The two-resistance isotope discrimination model (Eqn. (16)) has too many parameters to be
643 solved directly with the isotope data on hand. We have therefore made the simplifying
644 assumption that r_{wp} and r_{ch} are of the same magnitude when measured at a CO_2 concentration
645 of 400 µmol mol^{-1} and 1400 µmol m^{-2} s^{-1} *PAR*. The resistance across the cell wall and
646 plasmalemma was then calculated for each measured plant from Eqn. (15) with $\gamma = 1$ as

647 $$r_{wp} = \frac{r_m}{1 + V_c / A} ,$$

648 using the mesophyll resistance r_m estimated with the single-resistance model. r_{wp} was then
649 taken as a known constant used to calculate C_m values for all measurement conditions as

650 $$C_m = C_i - A r_{wp} .$$

651

652 **Data availability**

653 All generated and analyzed data that support the findings of this study are included in the
654 published article and its Supplementary Information.

655

References

1 Long, S. P., Farage, P. K. & Garcia, R. L. Measurement of leaf and canopy photosynthetic CO_2 exchange in the field. *J Exp Bot* **47**, 1629-1642, doi:10.1093/jxb/47.11.1629 (1996).

2 Busch, F. A., Sage, T. L., Cousins, A. B. & Sage, R. F. C_3 plants enhance rates of photosynthesis by reassimilating photorespired and respired CO_2. *Plant, Cell & Environment* **36**, 200-212, doi:10.1111/j.1365-3040.2012.02567.x (2013).

3 Gong, X. Y., Tcherkez, G., Wenig, J., Schäufele, R. & Schnyder, H. Determination of leaf respiration in the light: comparison between an isotopic disequilibrium method and the Laisk method. *New Phytol* **218**, 1371-1382, doi:doi:10.1111/nph.15126 (2018).

4 Farquhar, G. D. & Richards, R. A. Isotopic composition of plant carbon correlates with water-use efficiency of wheat genotypes. *Funct Plant Biol* **11**, 539-552, doi:https://doi.org/10.1071/PP9840539 (1984).

5 Cerling, T. E. *et al.* Global vegetation change through the Miocene/Pliocene boundary. *Nature* **389**, 153-158, doi:10.1038/38229 (1997).

6 Broecker, W. S., Takahashi, T., Simpson, H. J. & Peng, T.-H. Fate of fossil fuel carbon dioxide and the global carbon budget. *Science* **206**, 409-418, doi:10.1126/science.206.4417.409 (1979).

7 Yakir, D. & Sternberg, L. d. S. L. The use of stable isotopes to study ecosystem gas exchange. *Oecologia* **123**, 297-311, doi:10.1007/s004420051016 (2000).

8 Farquhar, G. D., O'Leary, M. H. & Berry, J. A. On the relationship between carbon isotope discrimination and the intercellular carbon dioxide concentration in leaves. *Aust J Plant Physiol* **9**, 121-137 (1982).

9 Evans, J. R., Sharkey, T. D., Berry, J. A. & Farquhar, G. D. Carbon isotope discrimination measured concurrently with gas-exchange to investigate CO_2 diffusion in leaves of higher plants. *Aust J Plant Physiol* **13**, 281-292 (1986).

10 Ubierna, N. *et al.* Critical review: incorporating the arrangement of mitochondria and chloroplasts into models of photosynthesis and carbon isotope discrimination. *Photosynth Res* **141**, 5-31, doi:10.1007/s11120-019-00635-8 (2019).

11 Tcherkez, G. *et al.* On the $^{13}C/^{12}C$ isotopic signal of day and night respiration at the mesocosm level. *Plant, Cell & Environment* **33**, 900-913, doi:doi:10.1111/j.1365-3040.2010.02115.x (2010).

12 Cernusak, L. A., Marshall, J. D., Comstock, J. P. & Balster, N. J. Carbon isotope discrimination in photosynthetic bark. *Oecologia* **128**, 24-35, doi:10.1007/s004420100629 (2001).

13 Gu, L. & Sun, Y. Artefactual responses of mesophyll conductance to CO_2 and irradiance estimated with the variable *J* and online isotope discrimination methods. *Plant, Cell & Environment* **37**, 1231-1249, doi:10.1111/pce.12232 (2014).

14 Barbour, M. M., Ryazanova, S. & Tcherkez, G. in *Plant Respiration: Metabolic Fluxes and Carbon Balance* (eds Guillaume Tcherkez & Jaleh Ghashghaie) 143-160 (Springer International Publishing, 2017).

15 Flexas, J. *et al.* Rapid variations of mesophyll conductance in response to changes in CO_2 concentration around leaves. *Plant Cell Environ* **30**, 1284-1298, doi:10.1111/j.1365-3040.2007.01700.x (2007).
16 Vrábl, D., Vašková, M., Hronková, M., Flexas, J. & Šantrůček, J. Mesophyll conductance to CO_2 transport estimated by two independent methods: effect of variable CO_2 concentration and abscisic acid. *J Exp Bot* **60**, 2315-2323, doi:10.1093/jxb/erp115 (2009).
17 Hassiotou, F., Ludwig, M., Renton, M., Veneklaas, E. J. & Evans, J. R. Influence of leaf dry mass per area, CO_2, and irradiance on mesophyll conductance in sclerophylls. *J Exp Bot* **60**, 2303-2314, doi:10.1093/jxb/erp021 (2009).
18 Farquhar, G. D., von Caemmerer, S. & Berry, J. A. A biochemical model of photosynthetic CO_2 assimilation in leaves of C_3 species. *Planta* **149**, 78-90 (1980).
19 Warren, C. Estimating the internal conductance to CO_2 movement. *Funct Plant Biol* **33**, 431-442, doi:10.1071/fp05298 (2006).
20 Harley, P. C., Loreto, F., Dimarco, G. & Sharkey, T. D. Theoretical Considerations When Estimating the Mesophyll Conductance to CO_2 Flux by Analysis of the Response of Photosynthesis to CO_2. *Plant Physiol* **98**, 1429-1436 (1992).
21 Di Marco, G., Manes, F., Tricoli, D. & Vitale, E. Fluorescence parameters measured concurrently with net photosynthesis to investigate chloroplastic CO_2 concentration in leaves of *Quercus ilex* L. *J Plant Physiol* **136**, 538-543, doi:https://doi.org/10.1016/S0176-1617(11)80210-5 (1990).
22 van der Putten, P. E. L., Yin, X. & Struik, P. C. Calibration matters: On the procedure of using the chlorophyll fluorescence method to estimate mesophyll conductance. *J Plant Physiol* **220**, 167-172, doi:10.1016/j.jplph.2017.11.009 (2018).
23 Farquhar, G. D. & Cernusak, L. A. Ternary effects on the gas exchange of isotopologues of carbon dioxide. *Plant Cell Environ* **35**, 1221-1231, doi:10.1111/j.1365-3040.2012.02484.x (2012).
24 McNevin, D. B. *et al.* Differences in carbon isotope discrimination of three variants of D-Ribulose-1,5-bisphosphate carboxylase/oxygenase reflect differences in their catalytic mechanisms. *J Biol Chem* **282**, 36068-36076, doi:10.1074/jbc.M706274200 (2007).
25 Roeske, C. & O'Leary, M. H. Carbon isotope effects on enzyme-catalyzed carboxylation of ribulose bisphosphate. *Biochemistry* **23**, 6275-6284 (1984).
26 Guy, R. D., Fogel, M. L. & Berry, J. A. Photosynthetic fractionation of the stable isotopes of oxygen and carbon. *Plant Physiol* **101**, 37-47, doi:10.1104/pp.101.1.37 (1993).
27 Evans, J. R. & von Caemmerer, S. Temperature response of carbon isotope discrimination and mesophyll conductance in tobacco. *Plant, Cell & Environment* **36**, 745-756, doi:10.1111/j.1365-3040.2012.02591.x (2013).
28 Gillon, J. S. & Yakir, D. Internal conductance to CO_2 diffusion and $C^{18}OO$ discrimination in C_3 leaves. *Plant Physiol* **123**, 201-214, doi:10.1104/pp.123.1.201 (2000).
29 Igamberdiev, A. U. *et al.* Photorespiration contributes to stomatal regulation and carbon isotope fractionation: a study with barley, potato and arabidopsis plants deficient in glycine decarboxylase. *Photosynth Res* **81**, 139-152, doi:10.1023/B:PRES.0000035026.05237.ec (2004).

30 Lanigan, G. J., Betson, N., Griffiths, H. & Seibt, U. Carbon Isotope Fractionation during Photorespiration and Carboxylation in *Senecio*. *Plant Physiol* **148**, 2013-2020, doi:10.1104/pp.108.130153 (2008).
31 Rooney, M. A. *Short-term carbon isotopic fractionation in plants*, University of Wisconsin-Madison, (1988).
32 Ubierna, N., Holloway-Phillips, M.-M. & Farquhar, G. D. in *Photosynthesis: Methods and Protocols* (ed Sarah Covshoff) 155-196 (Springer New York, 2018).
33 Bathellier, C., Badeck, F.-W. & Ghashghaie, J. in *Plant Respiration: Metabolic Fluxes and Carbon Balance* (eds Guillaume Tcherkez & Jaleh Ghashghaie) 43-68 (Springer International Publishing, 2017).
34 Ubierna, N. & Farquhar, G. D. Advances in measurements and models of photosynthetic carbon isotope discrimination in C_3 plants. *Plant, Cell & Environment* **37**, 1494-1498, doi:10.1111/pce.12346 (2014).
35 O'Leary, M. H. Carbon isotope fractionation in plants. *Phytochemistry* **20**, 553-567, doi:10.1016/0031-9422(81)85134-5 (1981).
36 Tcherkez, G., Farquhar, G., Badeck, F. & Ghashghaie, J. Theoretical considerations about carbon isotope distribution in glucose of C_3 plants. *Funct Plant Biol* **31**, 857-877, doi:https://doi.org/10.1071/FP04053 (2004).
37 Tcherkez, G., Mahé, A. & Hodges, M. $^{12}C/^{13}C$ fractionations in plant primary metabolism. *Trends Plant Sci* **16**, 499-506, doi:http://dx.doi.org/10.1016/j.tplants.2011.05.010 (2011).
38 von Caemmerer, S. & Farquhar, G. D. Some relationships between the biochemistry of photosynthesis and the gas exchange of leaves. *Planta* **153**, 376-387 (1981).
39 Tholen, D., Ethier, G., Genty, B., Pepin, S. & Zhu, X.-G. Variable mesophyll conductance revisited: theoretical background and experimental implications. *Plant, Cell & Environment* **35**, 2087-2103, doi:10.1111/j.1365-3040.2012.02538.x (2012).
40 Yin, X. & Struik, P. C. Simple generalisation of a mesophyll resistance model for various intracellular arrangements of chloroplasts and mitochondria in C_3 leaves. *Photosynth Res* **132**, 211-220, doi:10.1007/s11120-017-0340-8 (2017).
41 Tholen, D., Éthier, G. & Genty, B. Mesophyll conductance with a twist. *Plant, Cell & Environment* **37**, 2456-2458, doi:10.1111/pce.12401 (2014).
42 Tcherkez, G. *et al.* Leaf day respiration: low CO_2 flux but high significance for metabolism and carbon balance. *New Phytol* **216**, 986-1001, doi:10.1111/nph.14816 (2017).
43 Tcherkez, G. *et al.* Short-term effects of CO_2 and O_2 on citrate metabolism in illuminated leaves. *Plant, Cell & Environment* **35**, 2208-2220, doi:10.1111/j.1365-3040.2012.02550.x (2012).
44 Tcherkez, G., Mauve, C., Lamothe, M., Le Bras, C. & Grapin, A. The $^{13}C/^{12}C$ isotopic signal of day‐respired CO_2 in variegated leaves of *Pelargonium* × *hortorum*. *Plant, Cell & Environment* **34**, 270-283, doi:doi:10.1111/j.1365-3040.2010.02241.x (2011).
45 Schnyder, H., Schäufele, R., Lötscher, M. & Gebbing, T. Disentangling CO_2 fluxes: direct measurements of mesocosm-scale natural abundance $^{13}CO_2/^{12}CO_2$ gas exchange, ^{13}C discrimination, and labelling of CO_2 exchange flux components in controlled environments. *Plant, Cell & Environment* **26**, 1863-1874, doi:doi:10.1046/j.1365-3040.2003.01102.x (2003).

46 Wingate, L., Seibt, U., Moncrieff, J. B., Jarvis, P. G. & Lloyd, J. Variations in ^{13}C discrimination during CO_2 exchange by *Picea sitchensis* branches in the field. *Plant, Cell & Environment* **30**, 600-616, doi:10.1111/j.1365-3040.2007.01647.x (2007).
47 Gauthier, P. P. G. *et al.* In folio isotopic tracing demonstrates that nitrogen assimilation into glutamate is mostly independent from current CO_2 assimilation in illuminated leaves of *Brassica napus*. *New Phytol* **185**, 988-999, doi:10.1111/j.1469-8137.2009.03130.x (2010).
48 Tazoe, Y., von Caemmerer, S., Badger, M. R. & Evans, J. R. Light and CO_2 do not affect the mesophyll conductance to CO_2 diffusion in wheat leaves. *J Exp Bot* **60**, 2291-2301, doi:10.1093/jxb/erp035 (2009).
49 Ellsworth, P. V., Ellsworth, P. Z., Koteyeva, N. K. & Cousins, A. B. Cell wall properties in *Oryza sativa* influence mesophyll CO_2 conductance. *New Phytol* **219**, 66-76, doi:doi:10.1111/nph.15173 (2018).
50 Jahan, E., Amthor, J. S., Farquhar, G. D., Trethowan, R. & Barbour, M. M. Variation in mesophyll conductance among Australian wheat genotypes. *Funct Plant Biol* **41**, 568-580, doi:10.1071/FP13254 (2014).
51 Ubierna, N., Sun, W., Kramer, D. M. & Cousins, A. B. The efficiency of C_4 photosynthesis under low light conditions in *Zea mays*, *Miscanthus* x *giganteus* and *Flaveria bidentis*. *Plant, Cell & Environment* **36**, 365-381, doi:doi:10.1111/j.1365-3040.2012.02579.x (2013).
52 Douthe, C., Dreyer, E., Epron, D. & Warren, C. R. Mesophyll conductance to CO_2, assessed from online TDL-AS records of $^{13}CO_2$ discrimination, displays small but significant short-term responses to CO_2 and irradiance in *Eucalyptus* seedlings. *J Exp Bot* **62**, 5335-5346, doi:10.1093/jxb/err141 (2011).
53 Tcherkez, G. How large is the carbon isotope fractionation of the photorespiratory enzyme glycine decarboxylase? *Funct Plant Biol* **33**, 911-920, doi:https://doi.org/10.1071/FP06098 (2006).
54 Igamberdiev, A. U. *et al.* Decarboxylation of glycine contributes to carbon isotope fractionation in photosynthetic organisms. *Photosynth Res* **67**, 177-184, doi:10.1023/A:1010635308668 (2001).
55 Ivlev, A. A., Bykova, N. V. & Igamberdiev, A. U. Fractionation of carbon ($^{13}C/^{12}C$) isotopes in glycine decarboxylase reaction. *FEBS Lett* **386**, 174-176, doi:http://dx.doi.org/10.1016/0014-5793(96)00421-8 (1996).
56 Holloway-Phillips, M., Cernusak, L. A., Stuart-Williams, H., Ubierna, N. & Farquhar, G. D. Two-source $\delta^{18}O$ method to validate the $CO^{18}O$-photosynthetic discrimination model: implications for mesophyll conductance. *Plant Physiol* **181**, 1175-1190, doi:10.1104/pp.19.00633 (2019).
57 Farquhar, G. D. & Busch, F. A. Changes in the chloroplastic CO_2 concentration explain much of the observed Kok effect: a model. *New Phytol* **214**, 570-584, doi:10.1111/nph.14512 (2017).

Acknowledgements

We thank Nerea Ubierna and Guillaume Tcherkez for critical feedback on the manuscript. This work was supported by the Australian Government through the Australian Research Council Centre of Excellence for Translational Photosynthesis.

Author contributions

FAB conceived the study and FAB and GDF carried out the modelling. FAB and MMHP undertook the experimental work on a system set up by HSW and MMHP. The data were analyzed by MMHP and FAB. FAB wrote the manuscript with contributions from all authors.

Competing interests

The authors declare no competing financial interests.

Correspondence

Correspondence and requests for materials should be addressed to Florian A. Busch.

Figures

Figure 1 | Schematic representation of the model assumptions and its derivation. (a) Biochemical fractionations (associated with carboxylation (*b*), respiration (*e*), and photorespiration (*f*); red letters) assumed in the isotope discrimination model of Farquhar, et al. [8]. Assimilated CO_2, photorespiration and respiration all access one single pool of carbon, which contains a relative abundance of ^{13}C equal to the isotope ratio of the net assimilates *A* (R_A; double-bordered gray box). In this case, if R_d were to preferentially release light carbon, the heavy carbon left behind would increase the isotope ratio of the photorespired CO_2. (b) Schematic of the treatment of R_d as applied in the model described here. Assimilated CO_2 is in equilibrium with photorespired CO_2 via the carbon pool of the CBB cycle. The net assimilates are represented by the sum of two separate carbon pools: One pool consists of compounds that are synthesized without involving a decarboxylation step and therefore has the same carbon isotope ratio as the primary assimilates (dashed box; no R_d from biosynthesis). A second pool is made up of compounds, such as lipids and some amino acids, that require a decarboxylation step, which potentially fractionates (dashed box; R_d from biosynthesis). The model developed here assumes that the compounds of the second pool do not easily feed back into the CBB cycle and are therefore isotopically 'disconnected' from it. (c) Biochemical pathway of carbon assimilation within the cell outlining the calculation of the isotope ratios of individual metabolites (bold) and their fluxes. The labels in blue denote the average isotopic ratios of the associated metabolites in terms of the isotope ratio of RuBP (R_{RuBP}) and of the CO_2 at the site of carboxylation (R_{Cc}). Carbon entering or leaving the pathway is highlighted by

gray boxes. Letters in red indicate the fractionations *b*, *f*, and *e*, as well as the effective fractionation of the enzymes involved in the synthesis of triose-phosphates (TP) and their export from the CBB cycle (*h*). If the respiratory substrate is made up of 'old' carbon, as assumed here, there is no immediate connection between current TP carbon and respiration. To account for this, *e* needs to be replaced by $e' = e + e^*$ (see text for further explanation). For convenience we set $w = \frac{6C_c + 9\Gamma^*}{5C_c + 10\Gamma^*}$. RuBP: ribulose 1,5-bisphosphate; PG: 2-phosphoglycolate; PGA: 3-phosphoglycerate; $C_{(TP)}$: carbon in the form of TP; $C_{(OM)}$: carbon in the form of organic matter of the plant, which includes all non-carbohydrates.

Figure 2 | Mesophyll conductance (g_m) values estimated with different isotope discrimination models. The panels show CO_2 responses of g_m to C_i at 21% [O_2] measured with two sources of CO_2 with different isotopic composition using the old isotope model assuming R_d is isotopically connected to the CBB cycle (a, b) or the model derived here assuming R_d is isotopically disconnected (c, d). Both models were compared using the common simplification of *e** (a, c) or the implementation of *e** according to Eqn. (20) (b, d; see text), all with assumed values of *f* = 11‰ and *e* = -3‰. Only panel d, incorporating both model modifications, shows a close agreement of g_m values estimated with the two measurement gases. Average values are connected with lines for better discernibility only. n = 5 individual plants ± s.e.m.

Figure 3 | Separation of Δ^{13}_{obs} into its individual components. Calculations representing the values derived with the two different models using the implementation of *e** according to Eqn. (20) were made for the g_m/C_i responses shown in Fig. 2b and 2d. The discriminations associated

885 with Rubisco carboxylation (Δ_b), CO_2 diffusion through the boundary layer and stomata (Δ_{gb+gs}

886), CO_2 diffusion through the mesophyll (Δ_{gm}), respiration ($\Delta_{e'}$), and photorespiration (Δ_f) are

887 calculated using the old model assuming R_d is isotopically connected from the CBB cycle (a-e) or

888 the model derived here assuming R_d is isotopically disconnected (f-j), using values of f = 11‰

889 and e = -3‰ for both. Each panel compares the discrimination values obtained with the two

890 CO_2 source gases with different isotopic composition. Average values are connected with lines

891 for better discernibility. n = 5 individual plants ± s.e.m.

892

893 **Figure 4 | Key model parameters measured from C_i and *PAR*-responses.** Values shown are for

894 C_i-responses at 21% [O_2] (a, d, g, and j), C_i-responses at 2% [O_2] (b, e, h, and k), and PAR-

895 responses at 21% [O_2] (c, f, i, and l). The figure shows net CO_2 assimilation rate (A) and dark

896 respiration rate (R_d) (a-c), observed carbon isotope discrimination of the leaf (Δ^{13}_{obs}) (d-f), as

897 well as e^* values derived from measurements at $\delta_{CO2tank} = -7.0‰$ (g-i), and $\delta_{CO2tank} = -30.7‰$

898 (j-l). Note that e^* values are highly variable with measurement condition and differ when

899 calculated with the commonly used Eqn. (19) and Eqn. (20) suggested here. *PAR*:

900 photosynthetically active radiation. Average values are connected with lines for better

901 discernibility only. n = 5 individual plants ± s.e.m. for CO_2 responses and n = 4 individual plants ±

902 s.e.m. for light responses, except for 200 µmol m^{-2} s^{-1} *PAR*, where n = 3 individual plants ±

903 s.e.m..

904

905 **Figure 5 | Mesophyll conductance (g_m) values estimated with different discrimination**
906 **models.** Mesophyll conductance values were derived from measurements at $\delta_{CO2tank} = -7.0‰$
907 (a-c), and $\delta_{CO2tank} = -30.7‰$ (d-f) and estimated with the four possible combinations of R_d
908 being isotopically connected/disconnected with the CBB cycle, combined with the commonly
909 used simplification of e^* (Eqn. (19)) or calculating e^* according to Eqn. (20) taking into account
910 that Δ_{obs} changes with the environment. Note that the discrimination model treating R_d
911 isotopically disconnected in combination with e^* calculated according to Eqn. (20) yields
912 positive g_m values under all measurement conditions. For all panels f = 11‰ and e = -3‰ *PAR*:
913 photosynthetically active radiation. Average values are connected with lines for better
914 discernibility only. n = 5 individual plants ± s.e.m. for CO_2 responses and n = 4 individual plants ±
915 s.e.m. for light responses, except for 200 µmol m^{-2} s^{-1} *PAR*, where n = 3 individual plants ±
916 s.e.m..
917
918 **Figure 6 | The impact of the value of *f* on the estimated value of mesophyll conductance (g_m).**
919 Values in response to C_i are calculated with the old model assuming R_d is isotopically connected
920 from the CBB cycle (a-d) or the model derived here assuming R_d is isotopically disconnected (e-
921 h), using f = 0‰ (a, e), f = 7‰ (b, f), f = 13‰ (c, g), and f = -11‰ (d, h). For all panels e^* was
922 calculated according to Eqn. (20) and e = -3‰. Each panel compares the g_m values obtained
923 with the two CO_2 source gases with different isotopic composition. Average values are
924 connected with lines for better discernibility only. n = 5 individual plants ± s.e.m.
925

Figure 7 | Comparison of the apparent g_m derived assuming a single-resistance vs. a two-resistance discrimination model. The panels show values for C_i-responses at 21% [O_2] (a), C_i-responses at 2% [O_2] (b), and PAR-responses at 21% [O_2] (c) for measurements taken with $\delta_{CO2tank} = -7.01‰$. Solid symbols and lines are for values calculated with an isotope discrimination model assuming a single mesophyll resistance (Eqn. (13)) and open symbols and dashed lines with a model assuming two separate resistances across the cell wall and plasmalemma, and across the chloroplast envelope and stroma (Eqn. (16)). For the two-resistance case we assumed a fixed r_{wp} calculated as outlined in the Methods. e^* was implemented according to Eqn. (20) taking into account that Δ_{obs} changes with the environment, and we assumed the fractionation values e = -3‰, f = 7‰, and h = 0‰. n = 5 individual plants ± s.e.m. for CO_2 responses and n = 4 individual plants ± s.e.m. for light responses, except for 200 µmol m^{-2} s^{-1} *PAR*, where n = 3 individual plants ± s.e.m..

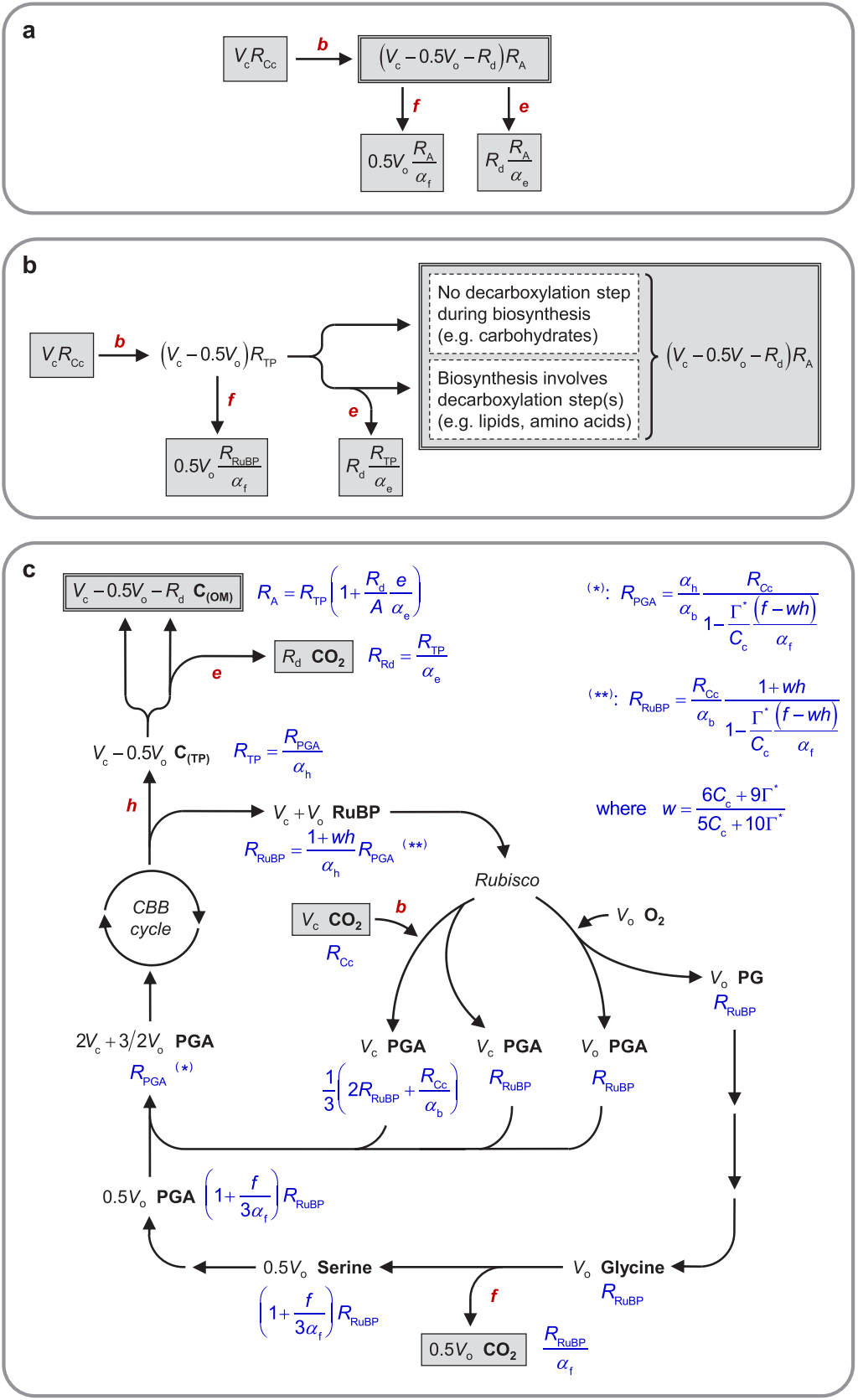
a
$V_c R_{Cc}$
b
$(V_c - 0.5V_o - R_d)R_A$
f
e
$0.5V_o \frac{R_A}{\alpha_f}$
$R_d \frac{R_A}{\alpha_e}$
b
$V_c R_{Cc}$
$(V_c - 0.5V_o)R_{TP}$
f
e
$0.5V_o \frac{R_{RuBP}}{\alpha_f}$
$R_d \frac{R_{TP}}{\alpha_e}$
No decarboxylation step during biosynthesis (e.g. carbohydrates)
Biosynthesis involves decarboxylation step(s) (e.g. lipids, amino acids)
$(V_c - 0.5V_o - R_d)R_A$
c
$V_c - 0.5V_o - R_d$ C(OM)
$R_A = R_{TP}\left(1 + \frac{R_d}{A}\frac{e}{\alpha_e}\right)$
e
R_d CO2
$R_{Rd} = \frac{R_{TP}}{\alpha_e}$
$V_c - 0.5V_o$ C(TP)
$R_{TP} = \frac{R_{PGA}}{\alpha_h}$
h
$V_c + V_o$ RuBP
$R_{RuBP} = \frac{1+wh}{\alpha_h} R_{PGA}$ (**)
Rubisco
CBB cycle
V_c CO2
R_{Cc}
b
V_o O2
V_o PG
R_{RuBP}
$2V_c + 3/2V_o$ PGA
R_{PGA} (*)
V_c PGA
$\frac{1}{3}\left(2R_{RuBP} + \frac{R_{Cc}}{\alpha_b}\right)$
V_c PGA
R_{RuBP}
V_o PGA
R_{RuBP}
$0.5V_o$ PGA $\left(1 + \frac{f}{3\alpha_f}\right)R_{RuBP}$
$0.5V_o$ Serine
$\left(1 + \frac{f}{3\alpha_f}\right)R_{RuBP}$
V_o Glycine
R_{RuBP}
f
$0.5V_o$ CO2
$\frac{R_{RuBP}}{\alpha_f}$
(*): $R_{PGA} = \frac{\alpha_h}{\alpha_b}\frac{R_{Cc}}{1 - \frac{\Gamma^*}{C_c}\frac{(f-wh)}{\alpha_f}}$
(**): $R_{RuBP} = \frac{R_{Cc}}{\alpha_b}\frac{1+wh}{1 - \frac{\Gamma^*}{C_c}\frac{(f-wh)}{\alpha_f}}$
where $w = \frac{6C_c + 9\Gamma^*}{5C_c + 10\Gamma^*}$

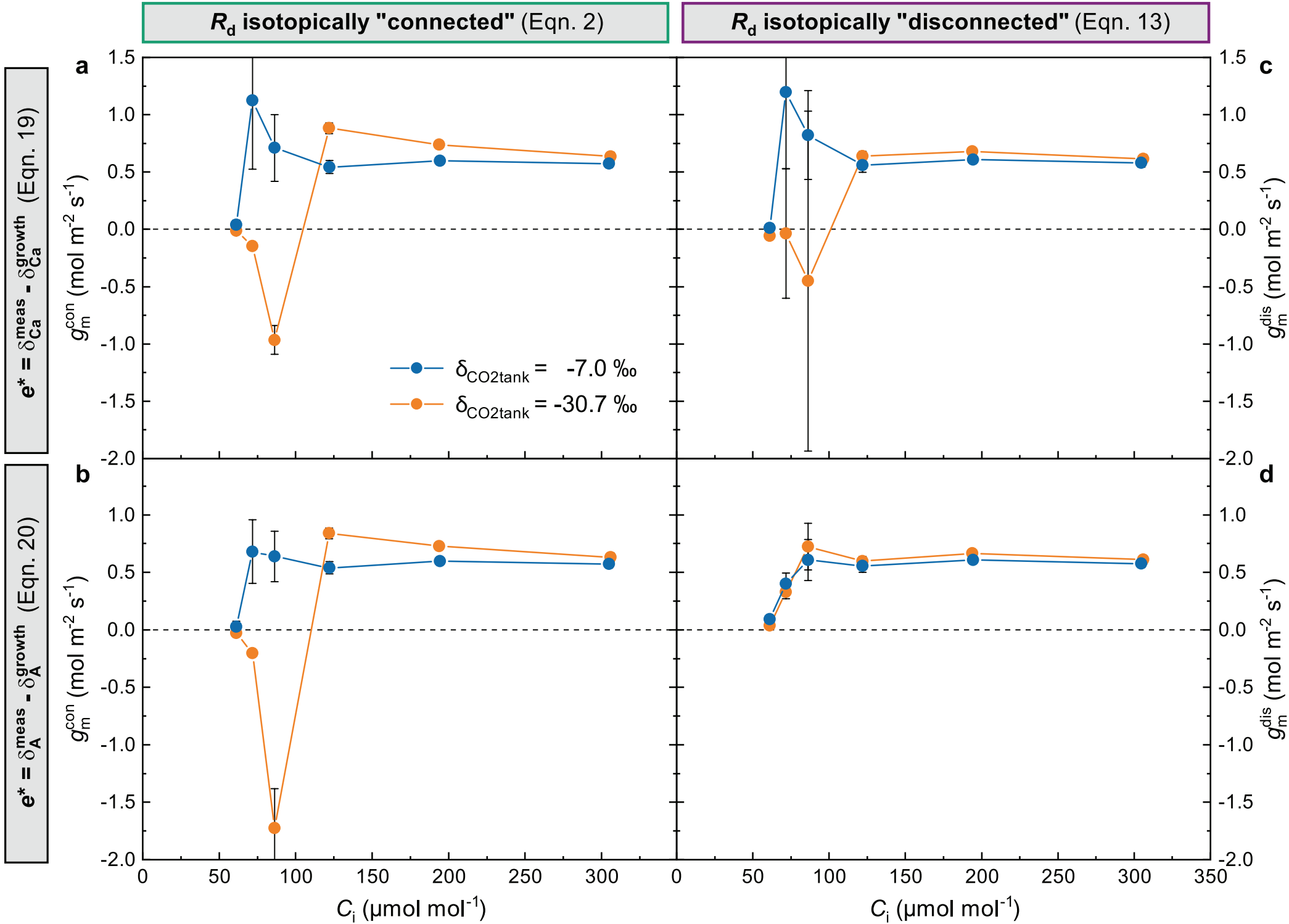
R_d isotopically "connected" (Eqn. 2)
R_d isotopically "disconnected" (Eqn. 13)
$e^* = \delta^{meas}_{Ca} - \delta^{growth}_{Ca}$ (Eqn. 19)
$e^* = \delta^{meas}_{A} - \delta^{growth}_{A}$ (Eqn. 20)
a
b
c
d
g_m^{con} (mol m^{-2} s^{-1})
g_m^{dis} (mol m^{-2} s^{-1})
C_i (µmol mol^{-1})
$\delta_{CO2tank}$ = -7.0 ‰
$\delta_{CO2tank}$ = -30.7 ‰

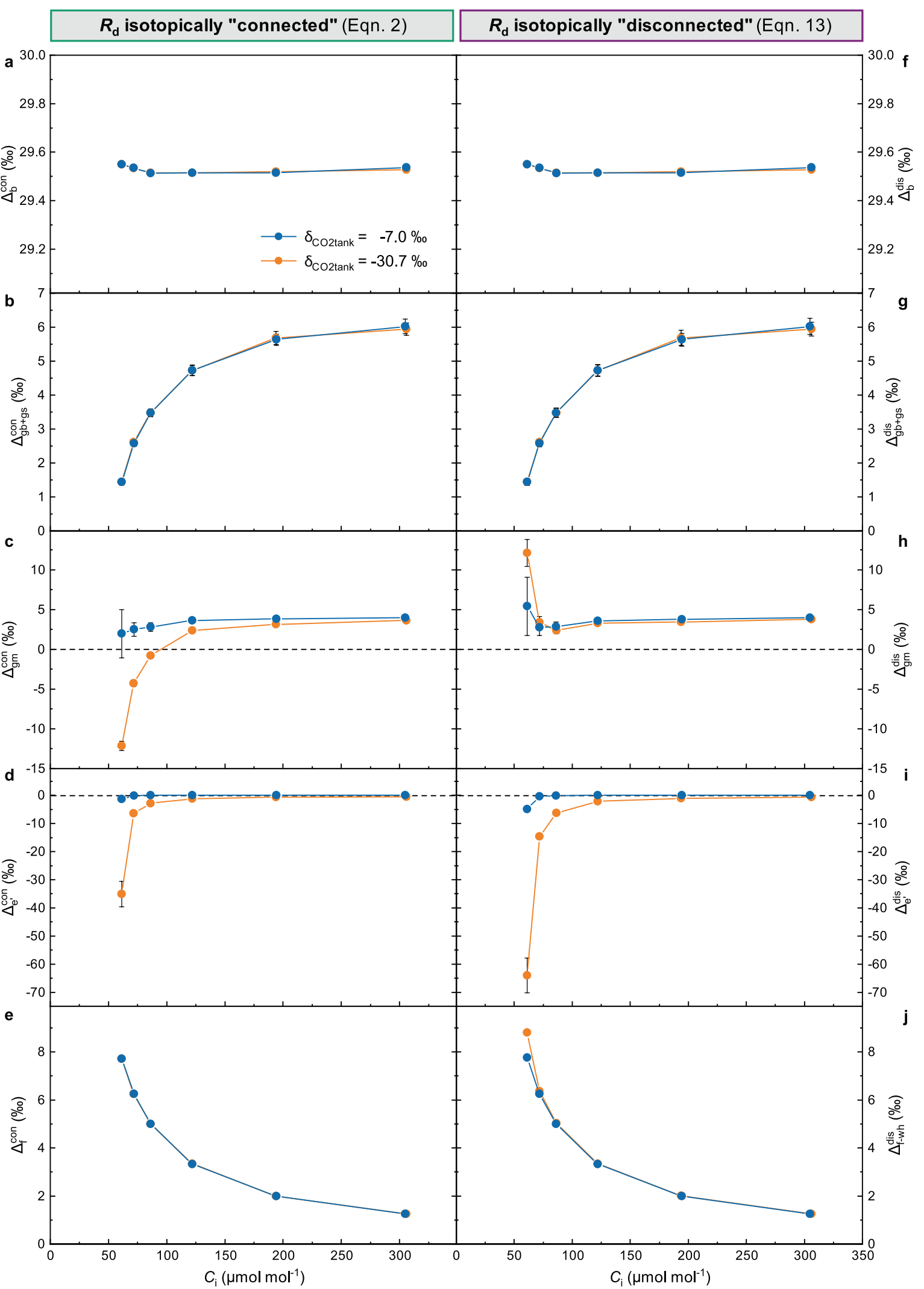
R_d isotopically "connected" (Eqn. 2)
R_d isotopically "disconnected" (Eqn. 13)
a
b
c
d
e
f
g
h
i
j
Δ_b^{con} (‰)
Δ_{gb+gs}^{con} (‰)
Δ_{gm}^{con} (‰)
$\Delta_{e'}^{con}$ (‰)
Δ_f^{con} (‰)
Δ_b^{dis} (‰)
Δ_{gb+gs}^{dis} (‰)
Δ_{gm}^{dis} (‰)
$\Delta_{e'}^{dis}$ (‰)
$\Delta_{f\text{-}wh}^{dis}$ (‰)
$\delta_{CO2tank}$ = -7.0 ‰
$\delta_{CO2tank}$ = -30.7 ‰
C_i (µmol mol^{-1})

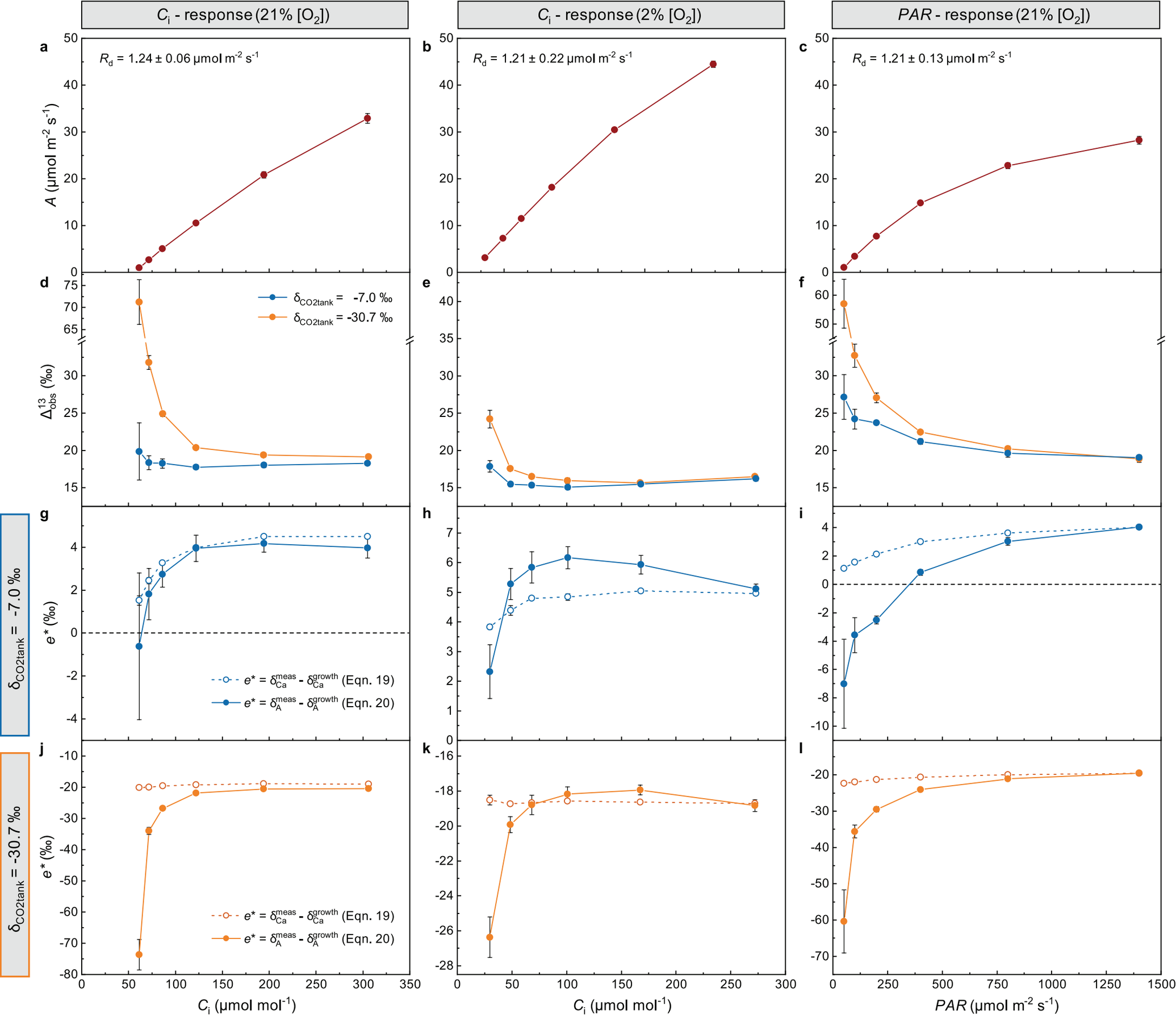
C_i - response (21% [O_2])
C_i - response (2% [O_2])
PAR - response (21% [O_2])
a
b
c
R_d = 1.24 ± 0.06 µmol m^{-2} s^{-1}
R_d = 1.21 ± 0.22 µmol m^{-2} s^{-1}
R_d = 1.21 ± 0.13 µmol m^{-2} s^{-1}
A (µmol m^{-2} s^{-1})
d
e
f
$\delta_{CO2tank}$ = -7.0 ‰
$\delta_{CO2tank}$ = -30.7 ‰
Δ^{13}_{obs} (‰)
g
h
i
$\delta_{CO2tank}$ = -7.0 ‰
*e** (‰)
$e^* = \delta^{meas}_{Ca} - \delta^{growth}_{Ca}$ (Eqn. 19)
$e^* = \delta^{meas}_{A} - \delta^{growth}_{A}$ (Eqn. 20)
j
k
l
$\delta_{CO2tank}$ = -30.7 ‰
*e** (‰)
$e^* = \delta^{meas}_{Ca} - \delta^{growth}_{Ca}$ (Eqn. 19)
$e^* = \delta^{meas}_{A} - \delta^{growth}_{A}$ (Eqn. 20)
C_i (µmol mol^{-1})
C_i (µmol mol^{-1})
PAR (µmol m^{-2} s^{-1})

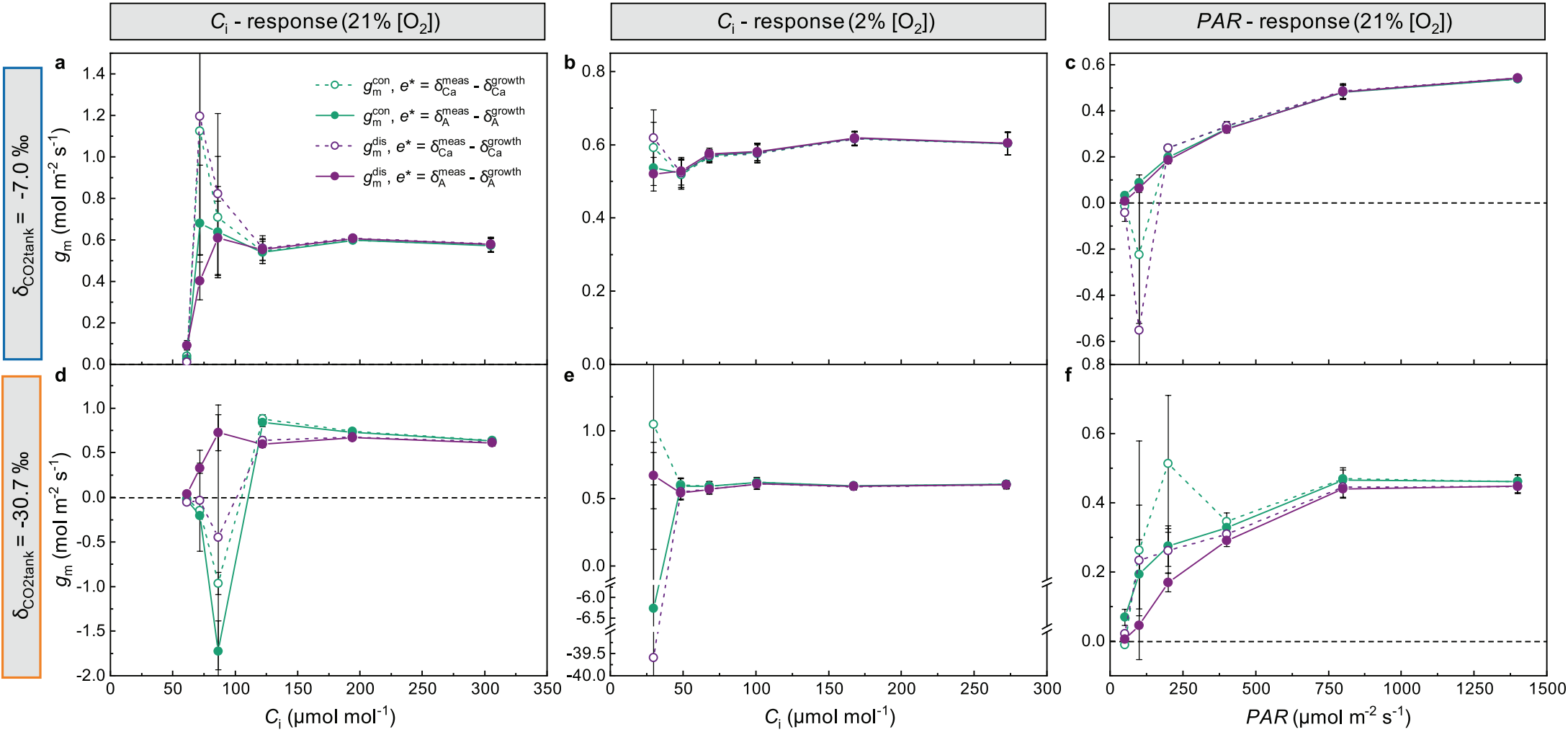
C_i - response (21% [O_2])
C_i - response (2% [O_2])
PAR - response (21% [O_2])
$\delta_{CO2tank}$ = -7.0 ‰
$\delta_{CO2tank}$ = -30.7 ‰
a
b
c
d
e
f
g_m^{con}, e^* = δ_{Ca}^{meas} - δ_{Ca}^{growth}
g_m^{con}, e^* = δ_{A}^{meas} - δ_{A}^{growth}
g_m^{dis}, e^* = δ_{Ca}^{meas} - δ_{Ca}^{growth}
g_m^{dis}, e^* = δ_{A}^{meas} - δ_{A}^{growth}
g_m (mol m^{-2} s^{-1})
C_i (µmol mol^{-1})
PAR (µmol m^{-2} s^{-1})

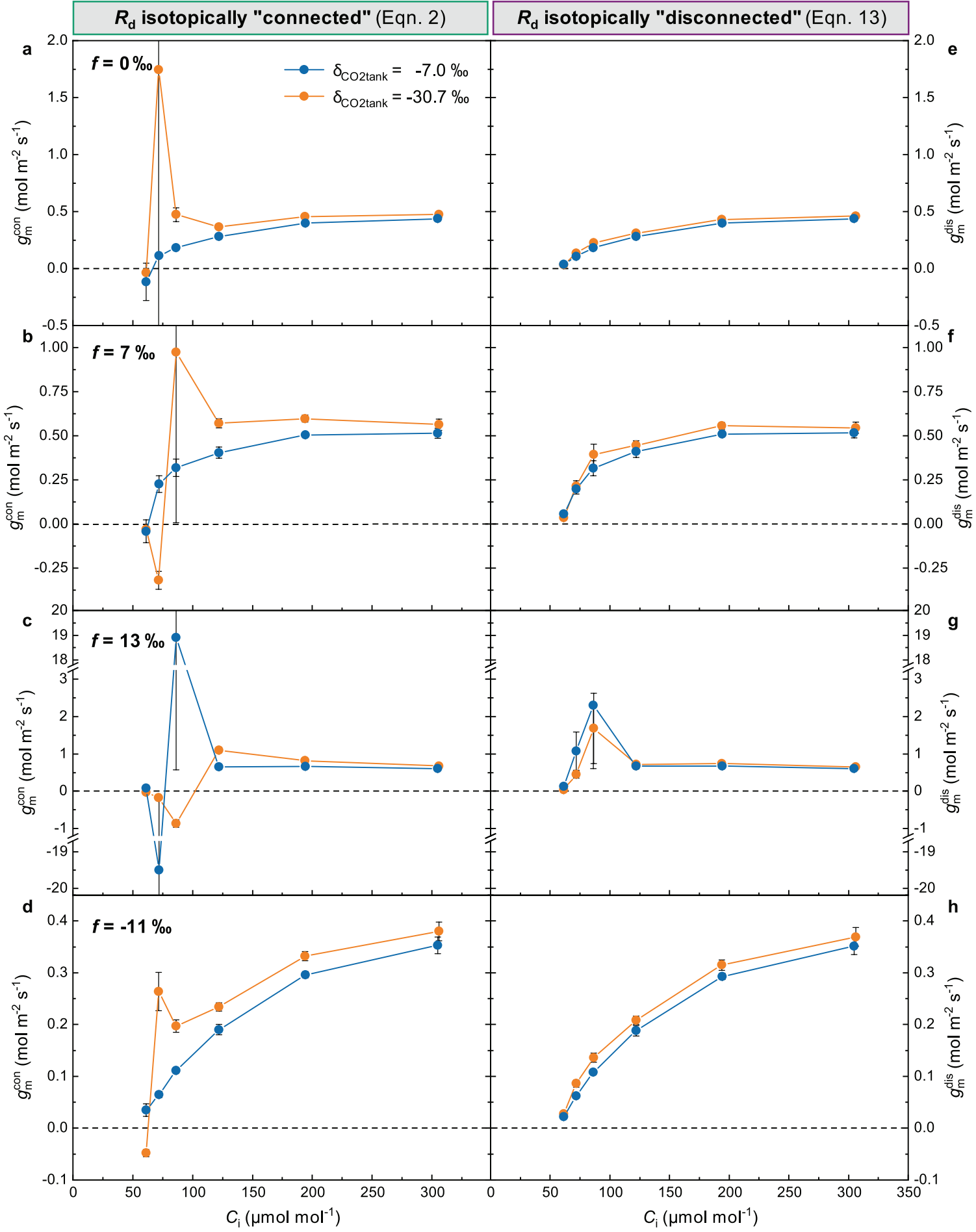
R_d isotopically "connected" (Eqn. 2)
R_d isotopically "disconnected" (Eqn. 13)
a
b
c
d
e
f
g
h
f = 0 ‰
f = 7 ‰
f = 13 ‰
f = -11 ‰
$\delta_{CO2tank}$ = -7.0 ‰
$\delta_{CO2tank}$ = -30.7 ‰
g_m^{con} (mol m^{-2} s^{-1})
g_m^{dis} (mol m^{-2} s^{-1})
C_i (µmol mol^{-1})

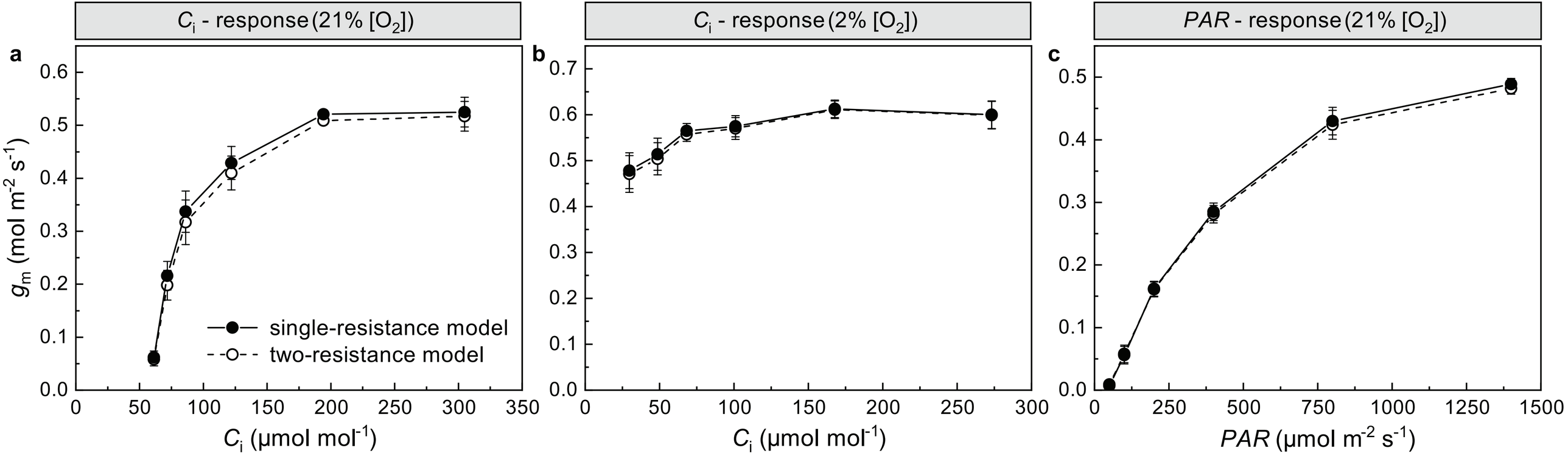
C_i - response (21% [O_2])
C_i - response (2% [O_2])
PAR - response (21% [O_2])
a
b
c
g_m (mol m^{-2} s^{-1})
single-resistance model
two-resistance model
C_i (μmol mol^{-1})
C_i (μmol mol^{-1})
PAR (μmol m^{-2} s^{-1})